AMERICAN SOCIETY FOR MICROBIOLOGY | mSystems

Check for updates

| Ecology | Research Article

Transcriptome remodeling drives acclimation to iron availability in the marine N_2-fixing cyanobacterium *Trichodesmium erythraeum* IMS101

Xin Zhong,[1] Ran Duan,[2] Shengwei Hou,[3,4] Meng Chen,[1] Xiaoming Tan,[5] Wolfgang R. Hess,[4] Tuo Shi[1,2]

AUTHOR AFFILIATIONS See affiliation list on p. 18.

ABSTRACT While enhanced phytoplankton growth as a result of iron (Fe) fertilization has been extensively characterized, our understanding of the underlying mechanisms remains incomplete. Here, we show in a laboratory setup mimicking Fe fertilization in the field that transcriptome remodeling is a primary driver of acclimation to Fe availability in the marine diazotrophic cyanobacterium *Trichodesmium erythraeum* IMS101. Fe supplementation promoted cell growth, photosynthesis and N_2 fixation, and concomitant expression of the photosynthesis and N_2 fixation genes. The expression of genes encoding major Fe-binding metalloproteins is tightly linked to cellular carbon and nitrogen metabolism and appears to be controlled by the ferric uptake regulator FurA, which is involved in regulating Fe uptake and homeostasis. This feedback loop is reinforced by substitutive expression of functionally equivalent or competitive genes depending on Fe availability, as well as co-expression of multiple Fe stress inducible *isiA* genes, an adaptive strategy evolved to elicit the Fe-responsive cascade. The study provides a genome-wide perspective on the acclimation of a prominent marine diazotroph to Fe availability, reveals an upgraded portfolio of indicator genes that can be used to better assess Fe status in the environment, and predicts scenarios of how marine diazotrophs may be affected in the future ocean.

IMPORTANCE The scarcity of trace metal iron (Fe) in global oceans has a great impact on phytoplankton growth. While enhanced primary productivity as a result of Fe fertilization has been extensively characterized, the underlying molecular mechanisms remain poorly understood. By subjecting the model marine diazotroph *Trichodesmium erythraeum* IMS101 to increasing concentrations of supplemented Fe, we demonstrate in it a comprehensively remodeled transcriptome that drives the mobilization of cellular Fe for coordinated carbon and nitrogen metabolism and reallocation of energy and resources. Our data provide broad genomic insight into marine diazotrophs acclimation to Fe availability, enabling the versatility and flexibility in choice of indicator genes for monitoring Fe status in the environment and having implications on how marine diazotrophs persist into the future ocean.

KEYWORDS *Trichodesmium*, iron limitation, transcriptome remodeling, *isiA* gene cluster, marine diazotroph

Cyanobacteria in the genus *Trichodesmium* are a prominent keystone N_2-fixing taxon (i.e., diazotroph) that dominates in tropical and subtropical oceans and play a crucial role in global carbon and nitrogen cycles (1–4). The abundance and distribution of *Trichodesmium* are affected by many environmental factors including temperature (5–7), pH (8–10), and nutrients (11, 12), particularly the content of trace metal iron (Fe) (13–15). In the vast majority of the world's open ocean, the concentration of dissolved

Editor Rachel Poretsky, University of Illinois Chicago, Chicago, Illinois, USA

Address correspondence to Tuo Shi, tuoshi@sdu.edu.cn, or Wolfgang R. Hess, wolfgang.hess@biologie.uni-freiburg.de.

Xin Zhong, Ran Duan, and Shengwei Hou contributed equally to this article. The author order was determined by drawing straws.

The authors declare no conflict of interest.

See the funding table on p. 19.

Received 8 November 2024
Accepted 17 February 2025
Published 17 April 2025

Fe that can be directly used is extremely low due to limited access to airborne dust and the oxidized state of seawater (16, 17). The concentration of dissolved inorganic Fe (dFe') in surface water is approximately only one-millionth of the concentration of plankton cells (i.e., one million cells competing for one Fe atom available) (18), which severely limits the primary productivity of phytoplankton. The impact of Fe limitation on phytoplankton growth has been confirmed by a dozen "Fe fertilization" mesocosm experiments deliberately performed in the high nutrient and low chlorophyll regions (19–23), as well as phytoplankton growth fueled by haphazard, natural events such as volcanic eruptions (24–26). Controlled laboratory experiments also demonstrated that Fe limitation severely inhibited the physiological activities of diatoms (27, 28), dinoflagellates (29, 30), coccolithophores (31, 32), and diazotrophic cyanobacteria including *Trichodesmium* and *Crocosphaera* (33–36).

Fe is an indispensable redox component of several essential cellular processes, including photosynthesis and N_2 fixation (37). In *Trichodesmium*, the simultaneous occurrence of these two processes during the light period (38) is puzzling, given their competition for intracellular Fe at the same time and the inhibition of nitrogenase by O_2 produced during photosynthesis. One plausible explanation is the spatial segregation between morphologically similar vegetative and diazotrophic cells within the filaments of the non-heterocystous *Trichodesmium* (38, 39) though true "diazocytes" have not been definitively identified to date (40, 41). Other mechanisms to protect nitrogenase may be involved, for example, photosynthetic proteins in nitrogenase-containing cells being inactive, RuBisCO acting as an oxygenase (photorespiration) at noon, and cytochrome oxidase driving rapid O_2 consumption (dark respiration) (40). Additionally, the potential presence of O_2 diffusion barriers (38), accumulation of antioxidants (42), ROS elimination through the Mehler reaction, and variability in the composition of phycobiliproteins (43) also play important roles in regulating photosynthesis during N_2 fixation. A recent study in natural populations of *Trichodesmium* has also shown that energy from photosynthesis can be shuttled directly to nitrogenase rather than to the glycogen production, thereby reducing the cells' density and sinking rate while enhancing their ability to acquire Fe from atmospheric dust particles (44).

Studies have demonstrated that *Trichodesmium* has evolved specific strategies to acquire and efficiently use Fe under Fe-limited conditions (45–48), such as changing colony morphologies to effectively collect Fe-rich dust particles (49, 50), sacrificing N_2-fixation to sustain photosynthesis (14), adjusting cell size and surface area (51), or reorganizing thylakoid membrane electron transport and changing cellular energy production pathways (52) to redistribute intracellular Fe resources. Proteomic analysis has revealed that changes in Fe availability reshape the Fe demand of *Trichodesmium*, resulting in approximately 50% less metabolic Fe needed under Fe-limited conditions (47), with some Fe-binding proteins being substituted by Fe-free equivalents (53). Transcriptomic analysis of both laboratory and field experiments has identified genes of Fe-stress biomarkers in N_2 fixation, photosynthesis, and Fe transport and storage, the expression of which is progressively changed with decreasing Fe availability (46, 54). In addition, research into the influence of iron, phosphorus, and ocean acidification on *Trichodesmium* and the unicellular marine N_2-fixing cyanobacterium *Crocosphaera* also shows that the diazotrophs could respond to the challenges posed by climate change and nutrient limitation at both transcriptional and translational levels (36, 53, 55, 56).

Despite the advances in previous studies, there remain many unanswered questions regarding *Trichodesmium* acclimation to Fe availability. Due to limited annotations of the *Trichodesmium* genome and a high number of genes of unknown functions, only a small number of biomarkers have so far been identified and characterized (54–56). Transcriptome-wide profiling of *Trichodesmium* response to variations in Fe availability may help open new avenues for searching genes and functions previously misannotated or overlooked. Moreover, the dynamic range of Fe concentrations in the future ocean is difficult to predict. For example, the drought and desertification driven by climate change, suboptimal agricultural activities, and the still increasing fossil fuel emissions are

all expected to significantly increase inputs of continental dust to much of the future ocean (57, 58), whereas the increasingly acidified seawater could affect the uptake of Fe by marine microbes by altering the chelation degree of Fe with organic ligands (59). These circumstances suggest that marine diazotrophs such as *Trichodesmium* may have plastic regulatory mechanisms in response to the labile Fe concentrations in the environment, a topic that has not been fully explored. To address these issues, we cultivated the model marine diazotroph *Trichodesmium erythraeum* strain IMS101 (hereafter IMS101) under laboratory conditions mimicking open ocean Fe fertilization. By monitoring the physiological performance of IMS101 alongside transcriptomic analysis with the Illumina RNA-Seq platform, we found stimulated growth, photosynthesis and N_2 fixation in IMS101 with increased Fe availability, and a comprehensively remodeled transcriptome associated with the mobilization of cellular Fe for coordinated carbon and nitrogen metabolism and reallocation of energy and resources. The study provides not only a genome-wide perspective toward acclimation to Fe availability in *Trichodesmium* and other marine diazotrophs but also an up-to-date portfolio of Fe-responsive indicator genes that will facilitate the monitoring of Fe availability status in the changing marine ecosystem.

RESULTS

We set up a laboratory-controlled experiment to mimic the scenario of Fe fertilization in the field to investigate IMS101 acclimation to Fe availability. Three concentrations of $FeCl_3$ at 0, 10, and 100 nM complexed with 20 µM ethylenediaminetetraacetic acid (EDTA) were applied to represent the low (LFe), medium (MFe), and high (HFe) concentration Fe supplemented, respectively. The measured initial concentrations of dissolved Fe (dFe') were approximately 2, 5, and 10 nM for the stock media LFe, MFe, and HFe, respectively, and the concentrations of dFe' decreased with time during IMS101 growth (Fig. 1). While stringent trace metal clean techniques were not applied, we were able to properly manipulate Fe limitation and fertilization in the laboratory setting here, as seen from the significant differences in specific growth rate, consumption of dFe', and expression of the Fe stress genes across the Fe supplementation treatments (Fig. 1; Fig. S1). It is also worth noting that the dFe' concentration in the LFe medium was higher than the level in nature that is often critically limiting (60). However, given the much higher abundance of IMS101, the LFe culture can arguably be considered Fe-limited, explaining the observations in this study.

Physiological responses of IMS101 to Fe supplementation

Compared with the LFe (i.e., Fe-deplete) control, the chlorophyll *a* (Chl *a*)-based specific growth rates (µ) of IMS101 were 1.5 and 2 times increased under the MFe and HFe treatments, respectively. Similarly, the N_2 fixation rates were increased 1.5 to 2 times under Fe-replete conditions (MFe and HFe) (Fig. 1A). The maximum light utilization coefficient (α) and maximum photosynthetic rate (P_{max}) were 2.19–2.22 and 1.2–1.9 times increased under the MFe and HFe conditions, respectively (Fig. 1B). In addition, the *idiA (Tery_3377)* transcript levels were increased 3.7 and 3.9 times under the MFe and LFe treatments, respectively, relative to that under the HFe condition (Fig. 1C). The transcript levels of the *isiA* (*Tery_1667*) gene were increased 51 and 96 times under the MFe and LFe treatments, respectively (Fig. 1C). The consumption of Fe was the fastest in the HFe treatment and the slowest in the LFe treatment (Fig. 1D), suggesting that IMS101 can utilize Fe and the Fe consumption is positively correlated with growth rate.

Overall transcriptomic remodeling of IMS101

Using the high-throughput Illumina RNA-Seq sequencing technique, we performed genome-wide gene expression analysis in IMS101 corresponding to Fe supplementation (Table S1). Of the 4,989 protein-coding genes in the IMS101 reference genome (61) (https://www.ncbi.nlm.nih.gov/nuccore/CP000393.1/), a total of 199 genes were

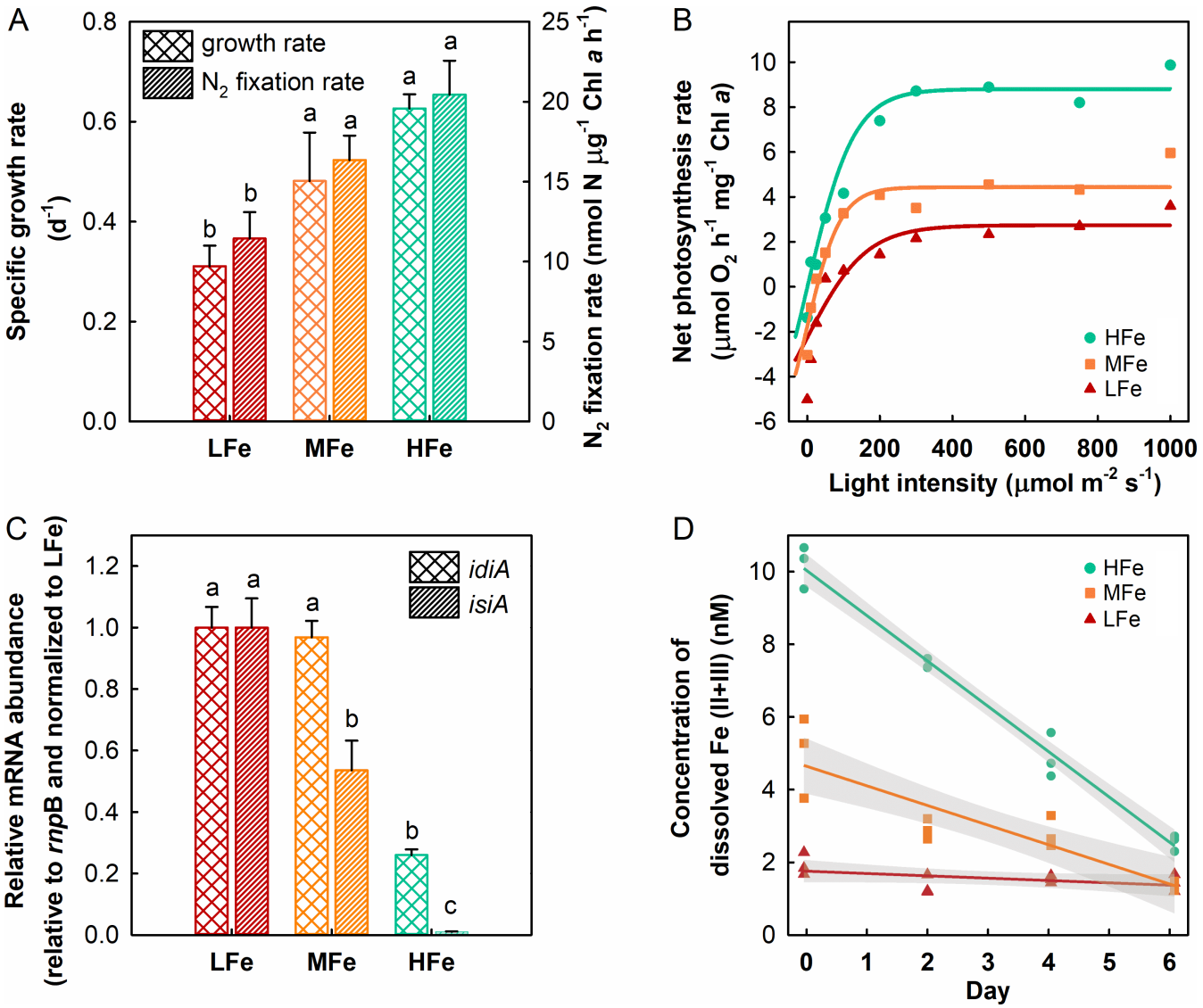

FIG 1 Physiological response of *T. erythraeum* IMS101 to increased iron availability. Shown are the chlorophyll-based specific growth rates and N_2 fixation rates (A), photosynthesis-irradiation curve fitted with the rates of oxygen evolution (B), relative mRNA abundances of two iron (Fe) stress indicator genes, *idiA* and *isiA* (C), and measured concentrations of dissolved Fe redox species (II + III) (dFe') in the culture media at designated time points during IMS101 growth (D). Measurements of N_2 fixation rates, photosynthetic O_2 evolution, and qPCR assay of Fe stress genes were conducted using samples collected on days 6, 7, and 5, respectively. IMS101 was grown in media supplemented with 0, 10, and 100 nM of $FeCl_3$ representing the low (LFe), medium (MFe), and high (HFe) concentration iron treatments, respectively. The data are plotted as mean ± standard deviation of biological triplicates (n = 3). Dissimilar lowercase letters in panels A and C represent significant differences across the treatments (P < 0.05). The shaded area in panel D represents the 95% confidence interval.

differentially expressed following the criterion of log_2-transformed fold change (log_2FC) >1 and adjusted P-value (padj) < 0.05 in the pairwise comparison between different treatments (Fig. S2; Table S2). The numbers of differentially expression genes (DEGs) under the HFe vs LFe, MFe vs LFe, and HFe vs MFe comparisons were 157, 90, and 63, respectively, and the numbers of up and downregulated genes across all comparisons were 113 and 86, respectively (Fig. 2; Fig. S3). In the HFe/LFe treatment comparison, the top 10 most significantly upregulated genes were the genes encoding small heat shock protein Hsp20 (*hsp20*, *Tery_3061/3062/3063/3064*), Fe-S binding ferredoxin (*fdxB*), cytochrome c_6 (*petJ*), B_{12}-independent methionine synthase (*metE*), H_2 uptake hydrogenases *hupL*, and hypothetical proteins Tery_1886 and Tery_0848, while the most significantly downregulated genes were the Fe stress gene *isiA* (*Tery_1667*) and its

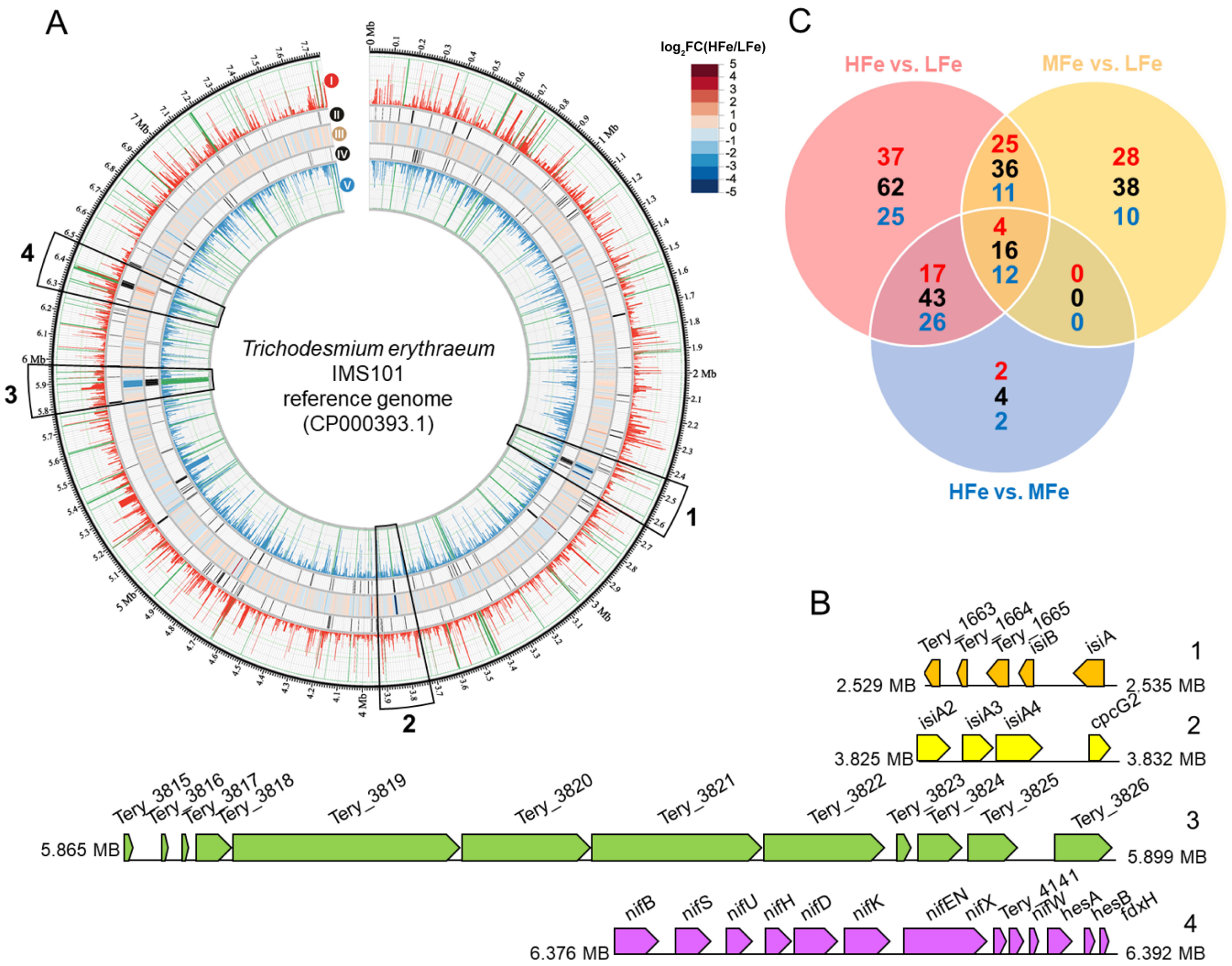

FIG 2 Transcriptome landscape of *T. erythraeum* IMS101 in acclimation to increased iron availability. (A) Circular presentation of differentially expressed genes between the HFe and LFe conditions along the IMS101 genome. The rings of the circos plot from the outermost to the innermost are (i) average read count per gene of the HFe treated samples, (ii) significantly upregulated genes under the HFe condition highlighted in dark color, (iii) heatmap of log_2FC between the HFe and LFe conditions, (iv) significantly downregulated genes under the HFe condition highlighted in dark color, and (v) average read count per gene of the LFe treated samples. For visualization purposes, a maximum read count of 50,000 has been set for rings i and v, and counts above this threshold are highlighted with green bars. Log_2FC, log_2-scaled fold change between the HFe and LFe treatments after normalization. (B) Close-up view of the four gene clusters depicted in panel A, the downregulated *isiAB* operon (1), *isiA2-isiA3-isiA4-cpcG2* (2), a cryptic gene cluster possibly involved in anti-microbial secondary metabolite biosynthesis (3), and the upregulated nitrogenase *nif* gene cluster (4). (C) Venn diagram summarizing the numbers of differentially expressed genes among treatments. Numbers in black represent the number of genes with >2-fold changes. From these, the numbers of upregulated genes are shown in red and those of downregulated genes in blue.

homologs (*isiA*-like, *Tery_2483/Tery_2484/Tery_2485*), a gene cluster of putative transcriptional regulators (*Tery_1663/1664/1665*), and genes encoding fructose-1,6-bisphosphate aldolase (*fbaAI*), phycobilisome linker polypeptide *cpcG2* (*Tery_2486*), and hypothetical protein Tery_1686 (Fig. S3 and S4). Compared with the LFe control, transcript levels decreased by 70% and 99% for *idiA* and *isiA* genes, respectively, in response to the HFe treatment (Table S2), which was consistent with the qPCR result (Fig. 1).

Expression of genes for Fe acquisition and homeostasis

The transcript level of *furA* encoding the global transcriptional regulator of intracellular Fe homeostasis increased twofold, whereas that of the other Fe homeostasis

regulator gene *furC* decreased by 86% in the HFe treatment relative to the LFe control (Fig. 3A). Transcription of the genes for ferric (*futA*/*idiA*, *futBC*) and ferrous (*feoAB*) Fe transport was also significantly downregulated. Transcript levels of genes coding for proteins with hemolysin-type calcium-binding (HTCaB)-like domains putatively involved in extracellular particulate Fe absorption (*Tery_0419*, *Tery_0424*, *Tery_2055*, and *Tery_2710*), and siderophore absorption system (*fhuD_3943, exbD_4449, tonB_2593*) (46, 47, 53) decreased upon the HFe treatment (Fig. 3B; Table S1). The two sets of Fe-S cluster assembly genes, i.e., the gene *iscS* and *iscA* and the *suf* operon *sufRBCDS*, showed opposite expression patterns, with *iscS* and *iscA* upregulated while *sufRBCDS* downregulated (Fig. 3C). To our expectation, the expression of two Fe storage genes, *ftn* encoding ferritin and *bfr* encoding heme-containing bacterioferritin, were both upregulated (Fig. 3D).

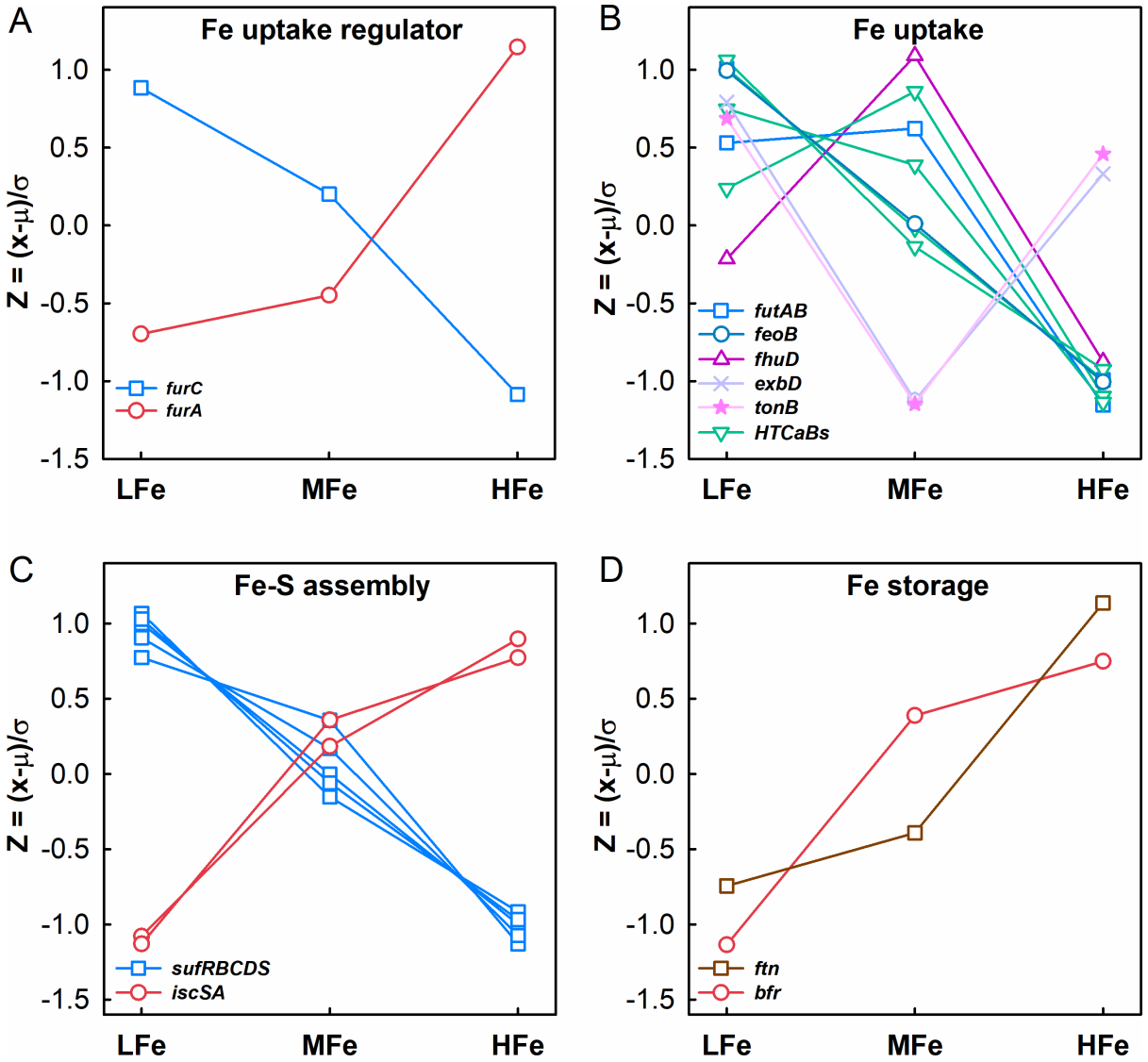

FIG 3 Changes in the expression of genes related to iron acquisition and utilization in *T. erythraeum* IMS101 upon iron supplementation. Shown are genes for Fe homeostasis regulatory factors (A), Fe absorption and acquisition (B), Fe-S cluster assembly (C), and Fe storage (D). The relative abundance of gene transcripts at each Fe supplementation concentration was $\log_2$ transformed and plotted according to the formula $Z = (x - \mu)/\sigma$, where x is the mean of $\log_2$CPM in one treatment, μ is the mean of $\log_2$CPM values in all treatments, and σ is the standard deviation of the overall normal distribution curve. This formula centers and scales a variable to mean 0 and standard deviation 1, which ensures that the criterion for finding linear combinations of the predictors is based on how much variation they explain and, therefore, improves the numerical stability.

Expression of genes involved in carbon and nitrogen cycling

With the increase of supplemented Fe, almost all genes involved in N_2 fixation were upregulated (Fig. 4A), particularly those having a high iron demand, such as the *nifHDK* gene cluster. The *modAB* genes involved in the molybdate transport and the *hupSL* genes encoding H_2 uptake hydrogenase were also upregulated under the HFe treatment. On the contrary, the ammonia (*amt*), nitrate/nitrite (*nrt*), and urea (*urtABCDE*) transport genes, as well as the nitrate (*narB*) and nitrite (*nirA*) reductase genes were downregulated (Table S1).

In addition, the expression of genes coding for phycobilisome, PSII and PSI proteins, cyt c_6, ferredoxin-NADP$^+$ reductase, NAD(P)H dehydrogenase, cytochrome oxidase, ATP synthase, CO_2 concentrating enzymes, Calvin cycle enzymes, tricarboxylic acid cycle enzymes, and the ferredoxin-thioredoxin enzymes including ferredoxin-thioredoxin reductase (FTR), ferredoxin (FdxH/B), and thioredoxin (Trx) was also upregulated under Fe-replete conditions (Table S1). However, transcript levels of some genes decreased upon the HFe treatment. For example, the three copies of *psbA* gene encoding D1 protein, *psbA1* (*Tery_4763*), *psbA2* (*Tery_0182*), and *psbA3* (*Tery_0183*), were downregulated by 1.4, 3.5, and 2 times, respectively (Fig. 4B; Table S1). In addition, *fbaAI* encoding fructose-1,6-bisphosphate aldolase, *isiB* encoding flavodoxin, and *cpcG2* encoding the phycobilisome rod core linker protein were downregulated 74, 4, and 30 times, respectively. As expected, the iron stress-inducible gene *isiA* (*Tery_1667*) was downregulated about 100 times upon the HFe treatment. However, unexpectedly, the other three *isiA*-like gene copies (*Tery_2483*, *Tery_2484,* and *Tery_2485*) (Fig. 2 and 5) exhibited an over 300 times further lower transcript level, the largest change in gene expression among all the DEGs (Fig. 4B; Table S2).

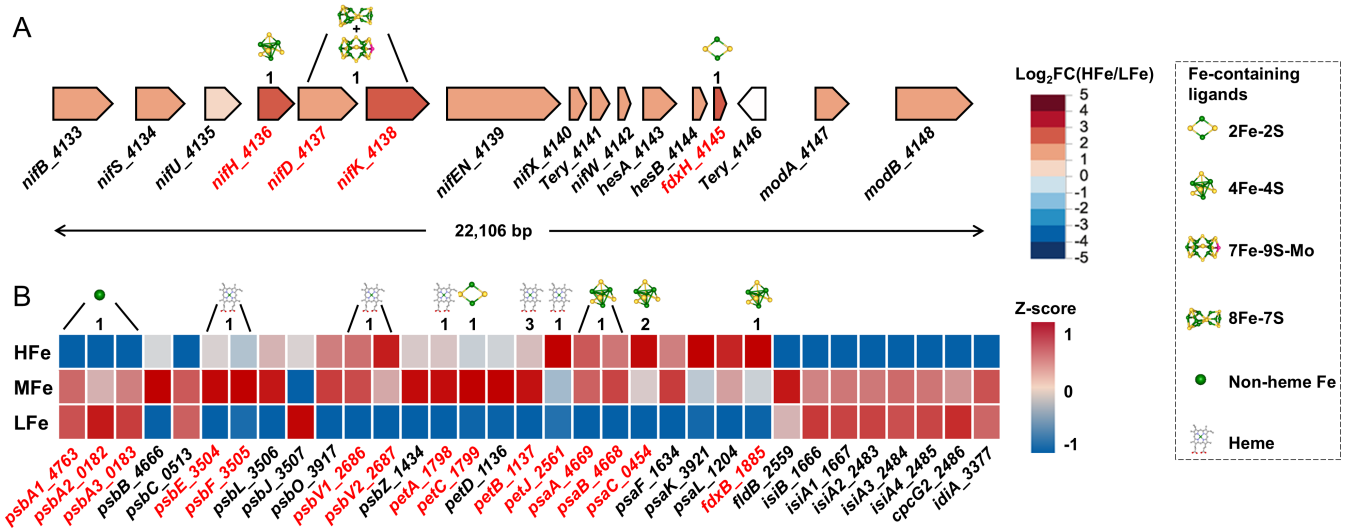

FIG 4 Photosynthetic and N_2-fixing genes differentially expressed upon iron supplementation. (A) Expression of genes involved in N_2 fixation is shown as fold changes in the level of transcripts between the HFe and LFe treatments. Also shown is the organization of genes in the 22,106 bp long *nif* gene cluster. (B) Expression of genes involved in photosynthesis is shown as *Z*-scores corresponding to each iron supplementation treatment. *Z*-scores were calculated according to the following formula: $Z = (x - \mu)/\sigma$, where x is the mean of $\log_2$CPM in one treatment, μ is the mean of $\log_2$CPM values in all treatments, and σ is the standard deviation of the overall normal distribution curve. Genes are labeled with gene symbol (if available) followed by locus tag of the open reading frame (e.g., *psbA1_4763* denoting the *psbA1* gene in the locus tag *Tery_4763* in the *Trichodesmium* genome). For the gene products associated with different forms of Fe (in red text), the numbers and types of the corresponding Fe ions/compounds are given. All Fe-containing molecules are shown in ball-and-stick representation with the Fe, S, Mo atoms depicted as green, yellow, magenta spheres, respectively.

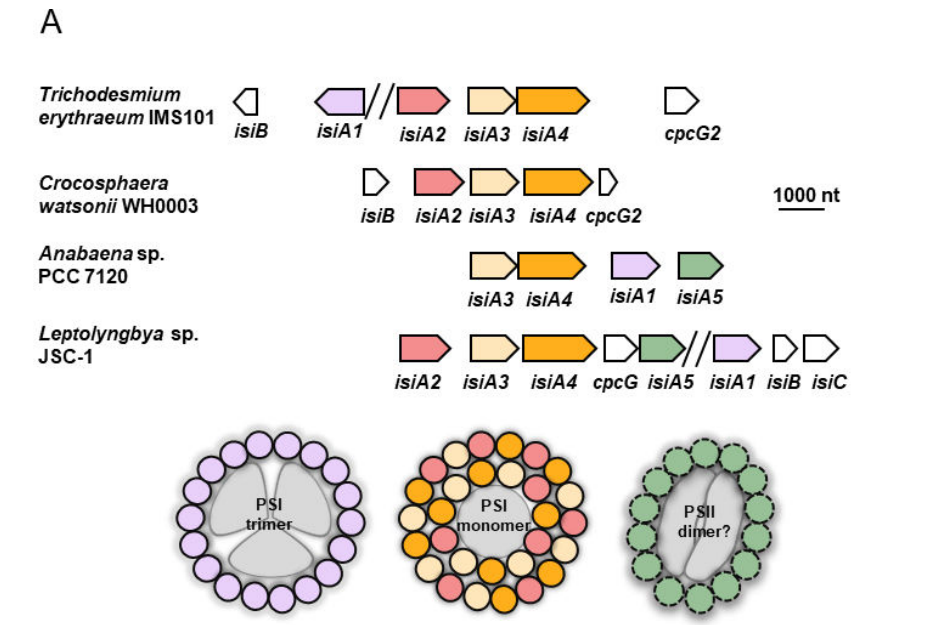

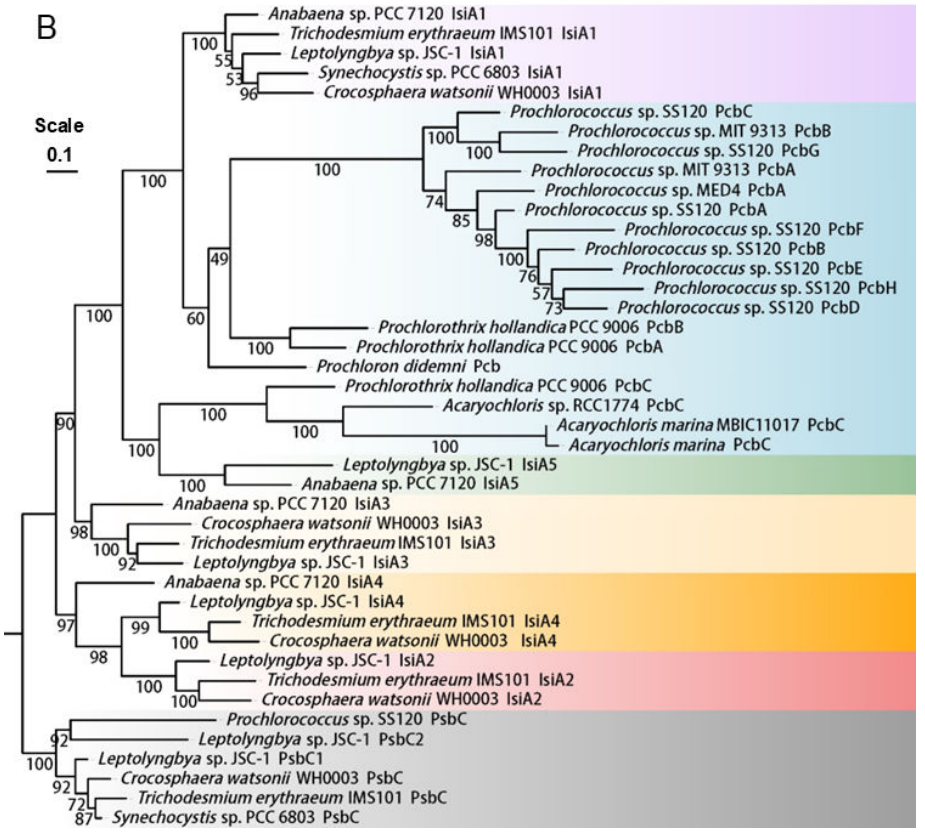

FIG 5 Diversity and conservation of *isiA* gene family in cyanobacteria. (A) Variants of *isiA* genes in *Trichodesmium erythraeum* IMS101, *Crocosphaera watsonii* WH0003, *Anabaena* sp. PCC7120 and *Leptolyngbya* sp. JSC-1 genomes, and their possible roles in the formation of super-complexes around photosystems under iron limitation conditions. Discontinued regions are marked with "//." (B) Maximum likelihood tree showing the phylogenetic relationship of *isiA*, *psbC,* and *pcb* genes found in diverse cyanobacteria. The phylogenic tree was constructed with IQ-TREE using aligned amino acid sequences of the IsiA homologs and was rooted with PsbC as the outgroup. Numbers at the branch denote the topological robustness of the tree evaluated by Bayesian criterion with 1,000 bootstrap replicates. Tree scale represents amino acid substitutions per site.

Expression of genes involved in chlorophyll *a*, heme, and vitamin B_{12} biosynthesis

Upon the HFe treatment, the expression of genes involved in heme *de novo* synthesis was upregulated by 2–3 times, while that of genes for vitamin B_{12} synthesis was downregulated by 60%–80% (Fig. 6). The two *cbiX* genes encoding cobaltochelatase also exhibited opposite expression patterns; *Tery_4741* was upregulated by 2 times, while *Tery_4427* was downregulated. So did the expression of the two genes encoding methionine synthase, with *metE* upregulated by 10 times, while *metH* downregulated (Fig. 7).

DISCUSSION

Our measurements of physiological parameters such as growth, photochemical efficiency, and N_2 fixation, coupled with the transcriptome sequencing analysis, unveiled the molecular mechanisms, whereby IMS101 acclimatizes to fluctuations in Fe availability. The strategic remodeling of gene expression in IMS101 mainly includes (i) upregulating Fe-demanding metabolic genes under Fe-replete conditions, (ii) enhancing light-harvesting capacity through upregulation of multiple iron stress genes under Fe-deplete conditions, (iii) substitutive expression of functionally equivalent genes depending on Fe availability, and (iv) mobilizing transcriptional regulators for the global Fe homeostasis and metabolic C/N balance.

Transcriptional upregulation of key metabolic genes in response to increased Fe availability

The three distinct metal prosthetic groups of nitrogenase alone require 19 Fe atoms (62). In IMS101 under Fe limitation, N_2 fixation is primarily downregulated in order to maintain the normal functions of other metabolic pathways (14, 47). Accordingly, with the increase in supplemented Fe in the culture media, the expression of almost all genes for N_2 fixation was upregulated, leading to enhanced nitrogenase activity (Fig. 1) and the production of ammonia (NH_3) and hydrogen (H_2). Transcription of the *hupSL* (*Tery_3369/3368*) gene cluster encoding the small and large subunits of the H_2 uptake hydrogenase (63) was upregulated under the HFe treatment (Table S2). The enhanced *hupSL* transcription can facilitate the reuse of H_2 by the H_2 uptake hydrogenase to regenerate electrons for various cell functions, as well as to produce ATP through oxyhydrogen reaction to minimize energy loss and O_2 damage to nitrogenase (64, 65). Moreover, transcription was also upregulated upon the HFe treatment for the key photosynthetic genes, including those encoding the PSII reaction center proteins (*psbB/E/F/L/O/V/Z*), cytochrome b_6f complex (*petCA*, *petBD*), PSI reaction center proteins (*psaA/B/C/F/L*), as well as the light-harvesting phycobilisomes (*cpcB*, *cpeB*, *apcA*) (Fig. 4 and 7). The presence of Fe-containing ligands is crucial for sustaining the structural integrity and proper functioning of the photosynthetic pathway. Indeed, Fe deprivation-induced transcriptional repression of these genes may restructure the photosynthetic pathway, leading to an increase in the PSII:PSI ratio (53) or conservation of intracellular Fe resources by altering ATP production pathways (e.g., via a short water-water cycle from PSII to a midstream oxidase or through electron transport from PSII to the respiratory terminal oxidase) (52).

Furthermore, the expression of genes encoding FTR (Tery_1567), Fdx (Tery_4145, Tery_1885), and Trx (Tery_1699) was upregulated under the HFe condition (Table S2). These proteins constitute the ferredoxin-thioredoxin system that converts the reducing power generated from light-activated electron transport in the thylakoid membrane into regulatory thiol signals in the stroma and hence impact the activities of several Calvin cycle enzymes (66). Although Fe is not required for enzymes involved in the Calvin cycle (52), the ensuing upregulation of these genes following the HFe treatment is probably a relief from the Fe stress in promoting the activities of Calvin cycle enzymes.

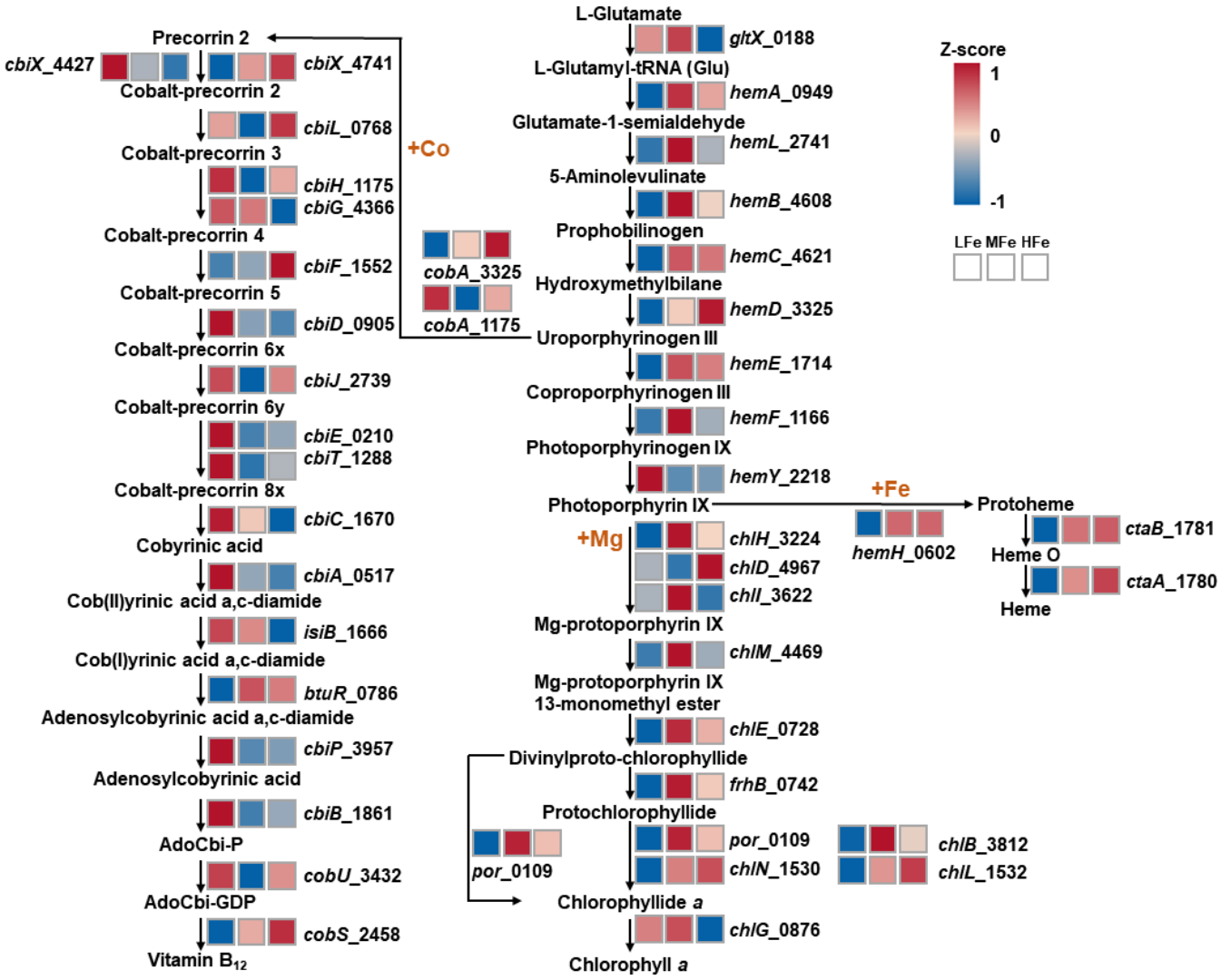

FIG 6 Expression of genes involved in the *de novo* synthesis of chlorophyll *a*, vitamin B_{12}, and heme upon iron supplementation. Most genes in the biosynthesis pathways of chlorophyll *a* and heme were significantly upregulated under the HFe treatment, while genes in the vitamin B_{12} biosynthesis pathway were significantly downregulated. Expression of genes is shown as *Z*-scores corresponding to each iron supplementation treatment. *Z*-scores were calculated according to the following formula: $z = (x - \mu)/\sigma$, where x is the mean of $\log_2$CPM in one treatment, μ is the mean of $\log_2$CPM values in all treatments, and σ is the standard deviation of the overall normal distribution curve. The genes are labeled with a gene symbol (if available) followed by a locus tag of the open reading frame (e.g., *chlM_4469* denoting the *chlM* gene in the locus tag *Tery_4469* in the *Trichodesmium* genome).

Enhancing light-harvesting capacity through the expansion of the *isiA* gene family

Intriguingly, our study revealed an *isiA*-like gene cluster *Tery_2483/2484/2485* (67) with the greatest expression change between the LFe and HFe treatments. This cluster is strikingly similar in gene sequence and synteny (Fig. 5A) to the *isiA2-isiA3-isiA4-cpcG2-isiA5* gene cluster in the freshwater cyanobacterium *Leptolyngbya* JSC-1, which was upregulated approximately 500 times under Fe limitation (68). While these additional IsiA-like copies are phylogenetically closely related to the *psbC*-encoded PSII reaction center core subunit CP43 (Fig. 5B), which is constitutively expressed (69, 70), they all lack the large loop on the lumenal side that is typical for CP43 (Fig. S5). It is, therefore, legitimate to clarify *Tery_2483*, *Tery_2484,* and *Tery_2485* as homologs (*isiA2*, *isiA3,* and *isiA4*) of the *isiA* gene (hereafter *isiA1*, *Tery_1667*), rather than *psbC* as currently annotated in the IMS101 genome. The PsaL domain at C-terminus of IsiA4 is suited to the formation of IsiA loops around PSI monomer while inhibiting PSI oligomerization (68, 71).

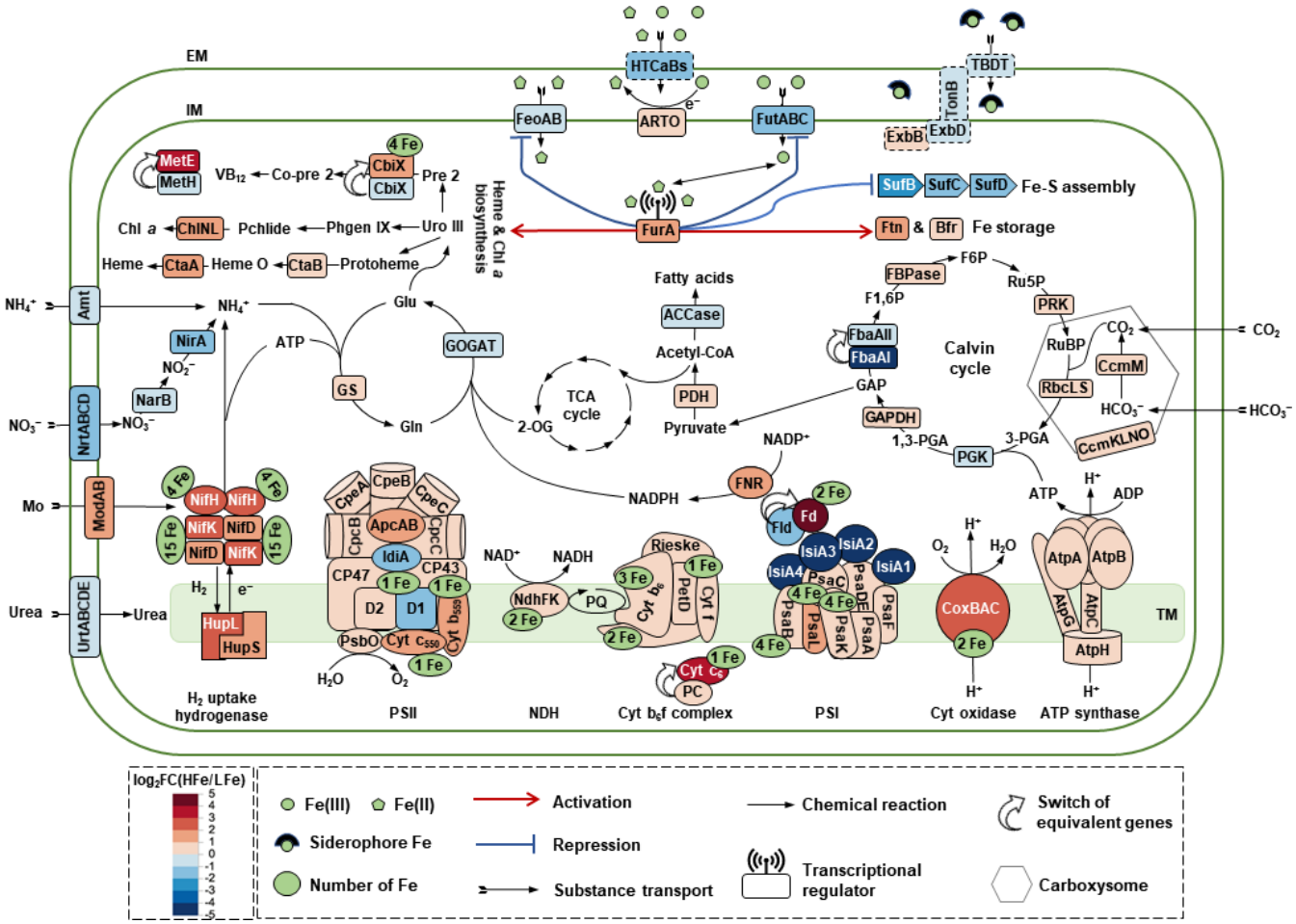

FIG 7 Schematic diagram illustrating significantly regulated gene products for coordinated nutrient transport and carbon and nitrogen metabolism in *T. erythraeum* IMS101 in acclimation to increased Fe availability. Fe supplementation promotes the expression of the genes encoding major Fe-binding metalloproteins involved in photosynthetic electron transport and structural subunits of the nitrogenase complex. The upregulated photosynthesis and N_2 fixation are accompanied by a balance between the central carbon and nitrogen metabolism, which is tightly linked through the GS-GOGAT cycle. The Fe redox is primarily under the control of the ferric uptake regulator FurA that functions as a transcriptional repressor of genes for Fe utilization, specifically those encoding the transporters of extracellular particulate (HTCaBs) and siderophore (FhuD) Fe, the plasma membrane transporters of ferric (FutABC) and ferrous (FeoAB) Fe, and the Fe-S cluster assembly proteins (SufBCDS). FurA also, possibly indirectly, functions as an activator in controlling the expression of genes encoding Fe storage ferritins (Ftn and Bfr) and proteins involved in heme and chlorophyll *a* biosynthesis. Moreover, the transcription of genes for nitrogen transport and utilization (*amt*, *nrtABCD*, *urtABCDE*, *narB*, and *nirA*) is likely under the control of a sophisticated network involving the Fur family. Proteins putatively involved in the extracellular particulate Fe-siderophore adsorption are boxed in dotted lines. Abbreviations are used as follows: TCA, tricarboxylic acid; Glu, glutamate; Gln, glutamine; GS, glutamine synthetase; GOGAT, glutamate synthase; Uro III, uroporphyrinogen III; Phgen IX, photoporphyrinogen IX; Chl *a*, chlorophyll *a*; Pchlide, Protochlorophyllide; Pre 2, precorrin 2; Co-pre 2, cobalt-precorrin 2; RuBP, ribulose-1,5-bisphosphate; 3-PGA, 3-phosphoglycerate; 1,3-PGA, 1,3-diphosphoglycerate; F1,6P, fructose-1,6-bisphosphate; F6P, fructose-6-phosphate; Ru5P, ribulose 5-phosphate; 2-OG, 2-oxoglutarate; EM, extracellular membrane; IM, intracellular membrane; TM, thylakoid membrane.

Transmission electron microscopic analysis suggests that IsiA1 may be involved in the formation of super-complex with trimeric PSI, while IsiA2/A3/A4 with monomeric PSI (68, 71). As a result, the number rises from a single ring of 17–18 IsiA copies surrounding PSI trimer (72) to double rings of 14–35 IsiA copies surrounding PSI monomer (73), which greatly enhances the light harvesting and energy transferring efficiency of the monomeric PSI-IsiA super-complex (68, 73).

The relative transcript change of *isiA2-isiA3-isiA4* was two times higher than that of *isiA1* (Table S2), suggesting that *isiA2-isiA3-isiA4* is more sensitive to Fe stress. Phylogenetic analysis showed that IsiA2, IsiA3, and IsiA4 each forms a monophyletic clade that is clearly distinct from IsiA1, implying that the expansion of IsiA2/A3/A4 may have

occurred independent of IsiA1, and likely emerged much later (e.g., after the great oxidation event) to facilitate acclimation to the worsening Fe limitation at geological timescales (Fig. 5B). This array of multiple *isiA* genes also exists in filamentous, heterocystous *Anabaena* sp. PCC 7120 and some of the unicellular marine diazotrophs such as *Crocosphaera* of large cell size (e.g., WH0003), but not small cell size (e.g., WH8501) (Fig. 5A). Under Fe-deficient conditions, cyanobacteria with multiple *isiA* genes have the advantage to accumulate IsiA products (71), resulting in reduced cellular content of the PSI reaction center and reduced levels of transcription of PSI core genes. Increased copies of *isiA* also contribute to higher photosynthetic efficiency in larger *Crocosphaera* under Fe limitation (74) and may be beneficial for low-light adapted *Synechococcus* ecotypes (75). Similarly, it is reasonable to speculate that *Trichodesmium* with multiple copies of *isiA* may exhibit superior performance in both light capture and photoprotection compared to those without.

Flexibility in substitutive gene expressions depending on Fe availability

The flexibility of cyanobacteria in acclimation to various environmental conditions can be achieved through the substitutive expression of different gene copies or genes encoding functionally equivalent proteins. In the former case, for example, Clarke et al. (76) found that in *Synechococcus* sp. PCC 7942, two different forms of D1 proteins (called D1:1 vs D1:2) vary in abundance between normal and high-irradiance photoinhibition conditions, as inferred from different patterns in the expression of their respective genes (i.e., *psbA1* for D1:1 and *psbA2*/3 for D1:2) (76). This regulation of gene expression of different *psbA* copies is executed so that *de novo* synthesis of D1 protein can be strictly controlled to maintain the stability of the photosynthetic apparatus under normal conditions or under environmental stress with a rapid turnover of D1 proteins (77). This pattern of *psbA* gene expression appeared to exist in IMS101 subjected to different concentrations of Fe supplemented (Table S1). Another example is the switch in expression between two copies of the gene encoding fructose-1,6-bisphosphate aldolase (FBA) in the Calvin cycle in IMS101 under Fe-replete conditions (Fig. 7; Table S1), where the expression of *Tery_1687* (*fbaAI*) encoding class I FBA (FbaAI) was replaced with that of *Tery_4099* (*fbaAII*) encoding Fe^{2+}-dependent class II FBA (FbaAII). The ratios of *fbaAI/fbaAII* transcription were 0.03 and 2.03 under the HFe and LFe treatments, respectively. This finding is consistent with those reported in diatoms (51, 78). Actually, because of the significant changes in the relative abundance of FbaAI and FbaAII under fluctuating Fe concentrations, the ratio of FbaAI/FbaAII is often used as an indicator for Fe availability (46, 47, 54). In addition, under the Fe-limited conditions, genes encoding Cu-containing plastocyanin (PC; Tery_2563) and flavodoxin (IsiB; Tery_1666) were upregulated to substitute Fe-containing cytochrome c_6 (Cyt c_6; Tery_2561) and ferredoxin (Fdx; Tery_4145), respectively. PC is crucial for phytoplankton in the open oceans where Cu is relatively abundant but Fe is scarce, and the replacement of Cyt c_6 by PC reduces the Fe requirement by roughly 10%, while the electron transport rates are still maintained at a high level (79).

There is also a trade-off in the synthesis of porphyrin compounds. Chl *a*, heme, and vitamin B_{12} are porphyrin-derived compounds with Mg, Fe, and Co as a ligand, respectively. Since the synthesis of chlorophyll and heme depends on Fe as a cofactor (80, 81), Fe deficiency in IMS101 may reduce the accumulation of chlorophyll and heme, causing more porphyrin precursors to be diverted to the vitamin B12 synthesis pathway by enhancing the absorption of Co (Fig. 6). A similarly negative relationship between Co concentrations in solution and intracellular Fe quota has been observed in *Microcystis aeruginosa* (82). Moreover, the increase in synthesis of vitamin B_{12} under LFe also activates the B_{12}-dependent methionine synthase (MetH; Tery_2492) to replace B_{12}-independent methionine synthase (MetE, Tery_0847) (Fig. 6 and 7). These results were consistent with the proteomics-based observation that MetE was more abundant under low B_{12} availability in the diatom *Phaeodactylum tricornutum* (83). It has also been found that phytoplankton preferentially uses MetH to save intracellular resources under

environmental stresses such as Fe limitation, as the expression of MetE will lead to a large consumption of resources and energy because the catalytic activity of MetE was about 100 times lower than that of MetH (1, 84). Furthermore, there are two copies of the *cbiX* gene in IMS101 encoding cobaltochelatase, which catalyzes cobalt insertion in vitamin B_{12} biosynthesis. Under high Fe concentrations, transcription of *cbiX1* (*Tery_4741*), which encodes a [4Fe-4S]-containing protein, was significantly upregulated compared to that of *cbiX2* (*Tery_4427*), whose gene product does not require the [4Fe-4S] ligand (85).

Global regulation for Fe homeostasis

In analogy to what has been established in other cyanobacteria, the regulator Fur family is involved in the global regulation of gene expression to maintain Fe homeostasis (86). The Fur family proteins include FurA, FurB, and FurC, which participate in Fe transport, biosynthesis, and cellular redox balance progresses. All the three Fur protein homologs exist in IMS101 (Fig. S6). Among them, FurC (PerR, Tery_3404) was found to be a metal-dependent H_2O_2 sensor (87), and the downregulation of *furC* upon the HFe treatment in our data indicated that the oxidative stress was relieved by Fe supplementation (Fig. 3A).

In IMS101 under Fe-replete conditions, the transcription of ferric uptake regulator FurA (Tery_1958) was induced, leading to tighter repression of Fe acquisition genes including the *feoAB* and *futABC* operons for transport of Fe^{2+} and Fe^{3+}, respectively (Fig. 7). Note that *feoAB* was consistently downregulated under both the MFe and HFe concentrations, whereas *futAB* was only downregulated upon the HFe treatment (Fig. 3B), suggesting that *Trichodesmium* cells prioritize Fe^{2+} absorption. Moreover, the expression of genes coding for Fe storage ferritins Ftn (Tery_4282) and Bfr (Tery_2787) was increased (Fig. 3D). These changes implied the role of FurA in controlling the expression of genes for Fe transport and storage to balance free Fe ion concentrations, which was also previously analyzed in the cyanobacteria *Synechocystis* sp. PCC 6803 (88) and *Anabaena* sp. PCC 7120 (89).

In addition, FurA could also be involved in the regulation of genes involved in the *de novo* synthesis of Fe-containing compounds such as the Fe-S clusters and hemes (Fig. 7) (90, 91). Three sets of genes, the *sufBCDS* (*Tery_4355/6/7/8*) gene cluster, *the nifU* (*Tery_4135*) *and nifS* (*Tery_4134*) genes, and the *iscS* (*Tery_4044*) and *iscA* (*Tery_3951*) genes are involved in Fe-S biosynthesis in *Trichodesmium* (90). The alternative regulation of these Fe-S assembly genes under varied Fe concentrations suggests the flexibility of *Trichodesmium* in acclimation to Fe availability. The *iscS* and *iscA* gene products are involved in general Fe-S cluster assembly (90), whereas *nifU* and *nifS* gene products only participate in the assembly of nitrogenase-specific Fe-S cluster (92, 93). These two systems were upregulated in IMS101 under the HFe treatment, possibly to meet the increasing demand for Fe-S cluster in fast-growing cells (Table S2). However, *sufBCDS* is usually induced by oxidative stress and Fe-restricted conditions to protect cells from ROS damage (94). In *Synechocystis*, the expression of the *sufBCDS* gene cluster is under the control of the transcriptional repressor SufR (95), an oxidative stress sensor that contains a [4Fe-4S] ligand for sensing the intracellular Fe level (96). Under Fe depletion, SufR loses its capacity for repression because the [4Fe-4S] ligand becomes scarce and the *sufBCDS* gene cluster would become highly expressed. In many bacteria, this conflict is solved by an sRNA regulator that is only transcribed under Fe starvation due to released repression from a FurA-controlled promoter (97, 98). For example, in *Synechocystis*, the sRNA IsaR1 post-transcriptionally represses *sufBCDS* (and several other genes) under the Fe limitation condition (98). Because a similar regulatory effect on the *sufBCDS* expression was not detected in this study (Fig. 7), such sRNAs may not exist in IMS101, pointing at a potentially remarkable difference in the regulatory machinery controlling the acclimation to low iron.

Another group of genes likely directly targeted by FurA are the iron stress protein-encoding gene *isiA1* (*Tery_1667*) and the flavodoxin-encoding *isiB* (*Tery_1666*), which were co-transcriptionally upregulated by 100 times and 4 times, respectively, under Fe

limitation (Fig. 4B; Table S2). In *Synechocystis*, Fur binds to the Fur box situated upstream of the *isiAB* operon, thus preventing the binding of RNA polymerase and inhibiting the transcription of *isiAB* under Fe-replete conditions (88, 99, 100). Putative Fur boxes for nine Fe-responsive genes (*isiAB*, *ftnA*, *feoA*, *hemD*, *hemH*, *futA*, *futC*, *ctaA*, and *bfr*) were identified in IMS101, and the sequences of these Fur binding sites are extremely conserved (Fig. S7). It is hence a strong evidence that FurA directly or indirectly regulates the transcription of these genes given the status of Fe availability (97).

It is worth noting that, due to limited annotations of the IMS101 genome and a high number of genes of unknown functions, the roles of many DEGs are unclear. For example, the *Tery_1663/1664/1665* gene cluster, encoding a putative Crp/Fnr family transcriptional regulator, a hypothetical protein, and a hydrolase (Fig. 2), was upregulated more than 100-fold at LFe (Table S2), but its regulatory mechanism is entirely uncharacterized. Vice versa, the four small heat shock protein genes (*hsp20*, *Tery_3061/3062/3063/3064*) were upregulated more than 10-fold under the HFe treatment (Fig. S3; Table S2), but their function in acclimation to Fe availability has not been experimentally addressed. One speculation is that under the nutritionally adequate conditions these chaperones are needed to bring the additionally synthesized protein into the correct conformation. What is even more intriguing is the cryptic polyketide synthase (PKS)-encoding gene cluster *Tery_3819/3820/3821/3822*, which was upregulated significantly under the LFe treatment (Fig. 2). Recent studies in *Escherichia coli* have shown the involvement of the pks island in synthesizing secondary metabolites with antimicrobial activity (101), some of which are implicated in prophage induction (102). *Trichodesmium* colonies are usually symbiotic with heterotrophic epibionts and other microorganisms including diatoms, proteobacteria, and other cyanobacteria (103–106). As the IMS101 culture was not stringently axenic in this study, some symbionts may assist the Fe absorption and storage of *Trichodesmium* under the HFe condition, while there is a competition between them for Fe utilization under the LFe condition. It is tempting to speculate that low Fe supply may result in increased synthesis of these antimicrobial metabolites, thereby favoring *Trichodesmium* colonization in interbacterial competition. A better characterization of these genes could potentially improve our understanding of their involvement in the cellular regulatory networks. In addition, the data set generated in this study can be further analyzed using other approaches, such as electron microscopic visualization of the IsiA-PSI/PSII super-complexes (68), epigenetic (107), or the proteomic (108) analysis of the DEGs. Meanwhile, protein modifications, such as acetylation and recombination in binding coenzymes and prosthetic groups, will influence enzymatic activity. Thus, a comprehensive analysis of transcriptomics, proteomics, metabolomics, and epigenomics might provide novel insight into *Trichodesmium* acclimation to Fe availability.

Conclusions

In this study, by subjecting *Trichodesmium erythraeum* IMS101 to increasing concentrations of supplemented iron (Fe), we observed enhanced growth, photosynthesis and N_2 fixation, and a concomitant remodeled transcriptome underpinning the physiological response of *T. erythraeum* IMS101 to increased Fe availability. Our data demonstrate the regulation of the Fe hemostasis by the transcriptional regulator FurA in controlling the expression of genes for Fe transport (e.g., *futABC* and *feoAB*), Fe storage as ferritin (*ftn*), and Fe-S assembly (*sufRBCDS*). Transcriptome profiling further unveils the plasticity in the transition of cellular processes for Fe resource allocation, for example, the substitutive switch between functionally equivalent genes and the trade-off between heme/Chl *a* and B_{12} biosynthesis depending on Fe availability. Moreover, the identification of the *isiA2/A3/A4* gene cluster expands our recognition of the iron stress gene *isiA*, suggesting that this gene family may have a more dynamic/plastic role than previously thought. Harboring multiple *isiA* copies, particularly in conjunction with genes for antimicrobial metabolites synthesis, may facilitate *Trichodesmium* to cope with more severe Fe deficiency to colonize the natural habitats. Furthermore, our study

provides broader genomic insight into the fundamental cellular processes responsible for acclimation to Fe availability in a representative, prominent marine diazotroph, given that IMS101 is frequently considered a model organism exhibiting unique characteristics. The identification of differentially expressed genes enables the versatility and flexibility in choice of indicator genes for monitoring fluctuations of Fe in the environment. Last but not least, our findings offer important implications for future studies on whether the adaptation mechanisms described here are applicable to other diazotrophs and marine bacteria in general, which is crucial for understanding their response to Fe limitation and how they persist into the future in an era of global climate change.

MATERIALS AND METHODS

Culture conditions and experimental design

Trichodesmium erythraeum strain IMS101 (hereafter IMS101) was obtained from the Provasoli-Guillard National Center for Marine Algae and Microbiota at Bigelow Laboratory (East Boothbay, Maine, USA) and grown in Aquil-tricho medium (109) prepared using surface natural seawater collected from the South China Sea at the South East Asia Time-series Study (SEATS, 18°N and 116°E) station. The bulk seawater was first filtered through a 2 µm pore size, 142 mm diameter polycarbonate filter membrane (Millipore, Bedford, MA, USA) to remove impurities, then autoclaved at 121°C for 20 min, and supplemented with $NaHCO_3$, KH_2PO_4, vitamins, and trace metals following the medium recipe. The medium was aliquoted into 2 L transparent polycarbonate bottles (Nalgene, Rochester, NY, USA), which were soaked in 1 N HCl overnight and thoroughly rinsed three times with ultrapure Milli-Q water before autoclaving.

IMS101 was cultivated at 26°C and 120 µmol quanta m^{-2} s^{-1} illumination under a 14 h:10 h light-dark cycle in 2 L transparent polycarbonate bottles (Nalgene, Rochester, NY, USA). Sterile fresh air was supplied to the culture medium with a syringe filter connected to an air pump. To choose the appropriate Fe supplementation concentrations, preliminary experiments were performed with 1, 10, 50, 100, and 200 nM $FeCl_3$ add ed into the prepared medium according to previous studies (56, 110). Based on the observed differences in IMS101 growth, a gradient of 0, 10, and 100 nM $FeCl_3$ complexed with 20 µM ethylenediaminetetraacetic acid (EDTA) was finally used to represent the low (LFe), medium (MFe), and high (HFe) Fe supplementation concentrations. To establish steady-state acclimation to differential Fe availability, IMS101 was routinely maintained in each of the LFe, MFe, and HFe media for up to 6 months under a semi-continuous mode (i.e., refreshed with the corresponding medium every 7 days). Cultures freshly diluted to ~1 µg L^{-1} of chlorophyll *a* (Chl *a*) content were used to start a new cycle of the Fe supplementation experiment, and the growth rates of *Trichodesmium* remain stable during the cultivation period (Fig. S1). Biologically triplicate samples (i.e., from different bottles) were collected and used for the following assays. As we cannot complete all the measurements in a single day, we had to sample at different days (but all at the midpoint of the light period). Samples for Chl *a* measurement were collected every other day. The rates of N_2 fixation, photosynthetic O_2 evolution, and quantitative PCR (qPCR) assays and transcriptomic sequencing were conducted using samples collected on days 6, 7, and 5, respectively.

Chl *a* extraction and calculation of specific growth rate

For Chl *a* extraction, 100 mL of algal culture for each Fe supplementation treatment was filtered on a 3 µm pore size, 25 mm diameter polycarbonate filter membrane (Millipore, Bedford, USA). The membrane was then soaked in 90% methyl alcohol and incubated at 65°C for 6 min. After centrifuging at 18,000 × *g* for 10 min, the supernatant was measured at the wavelengths of 650, 665, and 750 nm, and the light absorption values were recorded as A_{650}, A_{665}, and A_{750}, respectively. The Chl *a* concentration was calculated as

$$\text{Chl } a = 16.5 \times (A_{665} - A_{750}) - 8.3 \times (A_{650} - A_{750}) \times 2 \times 1,000/V,$$

where V was the volume of the algae, and the Chl *a*-derived specific growth rate (μ) was calculated as

$$\mu = \left[\ln(\text{Chl } a_t) - \ln\left(\text{Chl } a_{t_0}\right)\right]/(t - t_0),$$

where Chl a_t and Chl a_{t0} represent the concentration of Chl *a* at the time of t and t_0, respectively.

Measurement of photosynthetic O_2 evolution

Photosynthetic efficiency was assessed by measuring the rate of photosynthetic O_2 evolution using a Clark-type O_2 microsensor (Unisense, Aarhus, Denmark) suspended in 75 mL of algal cultures. The measurement temperature was set at 25°C and the actinic light intensities were set as 0, 10, 25, 50, 100, 200, 300, 500, 750, 1,000 μmol m^{-2} s^{-1} controlled by the light-emitting diodes. The rate of respiration was measured by keeping the algal cultures in the dark. The photosynthesis-irradiance (P-I) curves were obtained by fitting the data with the hyperbolic tangent model (111). The maximum light utilization coefficient α was given as the light-limited initial slope of the P-I curve, the net maximum photosynthetic rate P_{max} (μmol O_2 mg^{-1} Chl *a* h^{-1}) was recorded as the photosynthetic rate under light-saturated conditions, and the saturation irradiance E_k (μmol photons m^{-2} s^{-1}) was given as intercept between α and P_{max}.

Measurement of N_2 fixation rate

Samples were collected on day six at the midpoint of the photoperiod for measuring the N_2-fixation rate via acetylene reduction assay (112). Briefly, 5 mL of algal culture was added into 12 mL headspace vials (Labco, High Wycombe, UK), and 1 mL acetylene gas (>99%) was inserted into the bottle through the septum cap. A bottle of 5 mL pure culture medium was set as a blank. All the bottles were incubated for 2 h under the same condition as algal growth (see above). After the incubation, 100 μL $HgCl_2$ was immediately added to the bottles to stop the reaction and fix the samples. Five hundred microliters of gas samples was extracted with a gas injection needle (SGE, Sydney, Australia) and analyzed using a Clarus 580 gas chromatograph (Perkin Elmer, Waltham, MA, USA). The acetylene reduction rate was converted to N_2-fixation rate using a 4:1 molar ratio and normalized to Chl *a* content.

Measurement of soluble Fe concentrations

To minimize Fe contamination, trace metal grade ultrapure hydrochloric acid (HCl) (Merck, Germany) and ultrapure Milli-Q water (resistivity ≥ 18.2 MΩ cm) were used to clean the labware. Sampling was performed on an ultraclean workbench. Samples were taken at designated time points during the growth period (0, 2, 4, and 6 days after the inoculation). The IMS101 cultures were filtered on 0.2 μm pore size polycarbonate filter membranes. The filtrates were collected in 50 mL centrifuge tubes and acidified with HCl at a final concentration of 0.02% (wt/vol). Concentrations of dissolved Fe were measured using a custom-built flow analyzer as described by Chen et al. (113). Because EDTA was added in the culture medium, only unchelated, dissolved species of Fe (II + III) (dFe'), i.e., the bioavailable Fe, was detected.

RNA extraction

Samples for qPCR assays and transcriptomic sequencing were collected by filtering 700 mL of algal culture onto a 3 μm pore size 25 mm diameter polycarbonate membrane (Millipore, Bedford, MA, USA). Total RNA was extracted using the miRNeasy Mini Kit (Qiagen, Hilden, Germany) following the manufacturer's instructions. Briefly, the cells were lysed with QIAzol reagent, and chloroform was added to the cell homogenate. After

centrifugation, the homogenate was further separated into RNA-containing aqueous phase, DNA-containing interphase, and protein-containing organic phases. The aqueous supernatant was precipitated with 1.5 vol ethanol in an RNeasy Mini spin column, and the pellet was washed twice with the RPE buffer included in the kit. Total RNA was eluted by adding RNase-free water to the air-dried spin column and collected into a new collection tube via centrifugation. The content and quality of RNA were assessed using a NanoDrop spectrophotometer (Thermo Fisher Scientific, Waltham, MA, USA) which was calibrated with RNase-free water. Total RNA was treated with the TURBO DNA-free kit containing DNase and removal reagents (Ambion, Austin, TX, USA) following the manufacturer's protocol. The absence of genomic DNA was confirmed by PCR failing to amplify the 16S rRNA gene using the bacterial universal primers (114). The DNA-free RNA samples were kept at −80°C until further processing.

Quantitative PCR assay of Fe stress indicator genes

Reverse transcription of RNA samples was conducted using the PrimeScript RT reagent Kit with gDNA Eraser (Takara, Otsu, Japan). The reactions were prepared according to the manufacturer's instructions, and the reverse transcription steps (15 min at 37°C and 5 s at 85°C) were conducted using a T100 Thermal Cycler (Bio-Rad, Hercules, CA, USA). The TaqMan qPCR was performed according to Shi et al. (14). The cDNA amplification was conducted using the CFX96 Real Time PCR Machine (Bio-Rad, Hercules, CA, USA) with the following thermocycling steps: 50°C for 2 min and 95°C for 10 min at the initial denaturation stage, 95°C for 15 s and 60°C for 1 min at the cycling stage for 40 cycles. Transcript levels of the selected genes were normalized to *rnpB* using the $2^{-\Delta\Delta C_t}$ method, where C_t represented the number of cycles for genes to reach the threshold (115). Then, ΔC_t values of the HFe and MFe samples were normalized against that of the LFe samples to obtain the relative expression levels of *idiA* and *isiA*.

Transcriptomic sequencing and bioinformatics analysis

Total RNA samples were shipped on dry ice to Vertis Biotechnologie AG (Freising, Germany), where rRNA was depleted using the Ribo-Zero rRNA Removal Kit (Illumina, San Diego, CA, USA). Then, cDNA libraries were prepared according to the Illumina TruSeq protocol (Illumina, San Diego, USA). The transcriptome sequencing was performed on an Illumina NextSeq 500 platform. One of the replicate samples from the LFe and MFe treatments was not sequenced because of poor RNA extraction (i.e., $n = 2$ for LFe and MFe; $n = 3$ for HFe).

After demultiplexing, adapter sequences and low-quality bases of raw reads in fastq format were trimmed by atropos v1.1.18 (116) with parameters: -e 0.1 -Q 33 -q 20 --trim-n -m 30, and the quality was confirmed using FastQC v0.11.2 (117). PhiX174, sequencing artifacts and human genomic sequences were removed using bbduk.sh and bbmap.sh with parameters: minid = 0.95 maxindel = 3 bwr = 0.16 bw = 12 minhits = 2 qtrim = rl trimq = 10 untrim quick match fast, both scripts are part of the BBTools package v37.24 (available at https://jgi.doe.gov/data-and-tools/bbtools). Ribosomal RNA sequences were removed using SortMeRNA v2.0 (118) with default parameters, and the clean non-rRNA reads were aligned to the IMS101 reference genome using BWA MEM v0.7.12 (119) with default parameters. The number of reads aligned to each gene feature was counted using featureCounts v1.6.0 (120), and differentially expressed genes were called using DESeq2 v1.24.0 (121) with a $\log_2$ fold change ($\log_2$FC) cutoff of 1 and an adjusted *P*-value (padj) cutoff of 0.05. The RNA transcript levels were normalized using the default variance stabilizing transformation (vst) method implemented in DESeq2. The trimmed mean of *M*-value (TMM)-normalized read counts in counts per million (CPM) were also calculated using edgeR v3.26.8 (122) to compare gene expression across treatments (Table S1). GO and KEGG functional enrichment analyses were performed using GOstats v2.50 (123) and clusterProfiler v3.12 (124). Statistical analysis was done using R version

(3.6.1), and the R script used in this experiment has been uploaded to GitHub at https://github.com/hou-lab/Tricho-Transcriptomics/tree/main.

Phylogenetic analysis

Amino acid sequences of the IsiA and homologous proteins were aligned using MAFFT version 7.490 (125) with options -auto -maxiterate 1000. Ambiguously aligned regions were removed using trimAl version 1.4 (126) with the gappyout option. Maximum likelihood phylogenetic tree was built using IQ-TREE v2.2.0 (127) based on the best-fitting model automatically detected by ModelFinder (128) implementing the Bayesian information criterion using the -MFP option. Topological robustness of the tree was evaluated by 1,000 ultrafast bootstrap replicates. PsbC sequences were used as the outgroup.

ACKNOWLEDGMENTS

We thank Dalin Shi for providing the *Trichodesmium erythraeum* IMS101 strain, Thomas Bibby for stimulating discussions, Kunshan Gao, Naihao Ye, and Yitao Wang for the assistance with photosynthetic measurements, Yuanning Li and Hongyue Liu for phylogenetic analysis, and Yongming Huang for the measurement of soluble iron concentrations. We also thank the reviewers for their constructive comments that appreciably improve the manuscript.

This work was supported by the National Natural Science Foundation of China (41676092, 42076152).

T.S. conceptualized the study. W.R.H. participated in the study design. R.D. and X.Z. performed the experiments. X.T. and R.D. helped with logistics of samples preparation and shipment. X.Z., R.D., M.C., S.H., and T.S. analyzed the data. X.Z., T.S, R.D., S.H., M.C., and W.R.H. drafted and edited the manuscript. All authors read and approved the final version of the manuscript.

AUTHOR AFFILIATIONS

[1]Marine Genomics and Biotechnology Program, Institute of Marine Science and Technology, Shandong University, Qingdao, Shandong, China
[2]State Key Laboratory of Marine Environmental Science, College of Ocean and Earth Sciences, Xiamen University, Xiamen, Fujian, China
[3]Department of Ocean Science and Engineering, Southern University of Science and Technology, Shenzhen, Guangdong, China
[4]Genetics and Experimental Bioinformatics, Institute of Biology III, University Freiburg, Freiburg, Germany
[5]State Key Laboratory of Biocatalysis and Enzyme Engineering, Environmental Microbial Technology Center of Hubei Province, School of Life Sciences, Hubei University, Wuhan, Hubei, China

PRESENT ADDRESS

Ran Duan, Department of Biological Sciences, University of Southern California, Los Angeles, California, USA

AUTHOR ORCIDs

Xin Zhong http://orcid.org/0000-0002-6458-1436
Shengwei Hou http://orcid.org/0000-0002-4474-7443
Wolfgang R. Hess http://orcid.org/0000-0002-5340-3423
Tuo Shi http://orcid.org/0000-0003-3362-8163

FUNDING

Funder	Grant(s)	Author(s)
MOST | National Natural Science Foundation of China (NSFC)	41676092	Tuo Shi
MOST | National Natural Science Foundation of China (NSFC)	42076152	Tuo Shi

DATA AVAILABILITY

Raw sequence data for the transcriptome sequencing reported in this study have been deposited in the NCBI Sequence Read Archive under BioProject accession number PRJNA866334.

ADDITIONAL FILES

The following material is available online.

Supplemental Material

Supplemental Figures (mSystems01499-24-s0001.docx). Figures S1 to S7.
Table S1 (mSystems01499-24-s0002.xlsx). All processed data of normalized expression.
Table S2 (mSystems01499-24-s0003.xlsx). List of differentially expressed genes.

REFERENCES

1. Bergman B, Sandh G, Lin S, Larsson J, Carpenter EJ. 2013. *Trichodesmium*–a widespread marine cyanobacterium with unusual nitrogen fixation properties. FEMS Microbiol Rev 37:286–302. https://doi.org/10.1111/j.1574-6976.2012.00352.x
2. Capone DG, Burns JA, Montoya JP, Subramaniam A, Mahaffey C, Gunderson T, Michaels AF, Carpenter EJ. 2005. Nitrogen fixation by *Trichodesmium* spp.: an important source of new nitrogen to the tropical and subtropical North Atlantic Ocean. Global Biogeochem Cycles 19:GB2024. https://doi.org/10.1029/2004GB002331
3. Carpenter EJ, Romans K. 1991. Major role of the cyanobacterium *Trichodesmium* in nutrient cycling in the north atlantic ocean. Science 254:1356–1358. https://doi.org/10.1126/science.254.5036.1356
4. Capone DG, Zehr JP, Paerl HW, Bergman B, Carpenter EJ. 1997. *Trichodesmium*, a globally significant marine cyanobacterium. Science 276:1221–1229. https://doi.org/10.1126/science.276.5316.1221
5. Breitbarth E, Oschlies A, LaRoche J. 2007. Physiological constraints on the global distribution of *Trichodesmium* – effect of temperature on diazotrophy. Biogeosciences 4:53–61. https://doi.org/10.5194/bg-4-53-2007
6. Boatman TG, Lawson T, Geider RJ. 2017. A key marine diazotroph in a changing ocean: The interacting effects of temperature, CO_2 and light on the growth of *Trichodesmium erythraeum* IMS101. PLoS One 12:e0168796. https://doi.org/10.1371/journal.pone.0168796
7. Levitan O, Kranz SA, Spungin D, Prásil O, Rost B, Berman-Frank I. 2010. Combined effects of CO_2 and light on the N_2-fixing cyanobacterium *Trichodesmium* IMS101: a mechanistic view. Plant Physiol 154:346–356. https://doi.org/10.1104/pp.110.159285
8. Hutchins DA, Fu F-X, Zhang Y, Warner ME, Feng Y, Portune K, Bernhardt PW, Mulholland MR. 2007. CO_2 control of *Trichodesmium* N_2 fixation, photosynthesis, growth rates, and elemental ratios: implications for past, present, and future ocean biogeochemistry. Limnol Oceanogr 52:1293–1304. https://doi.org/10.4319/lo.2007.52.4.1293
9. Wu S, Yu K, Wang F, Mi T, Zhen Y. 2024. Impact of low pH/high pCO_2 on the physiological response and exopolysaccharide content in cyanobacteria *Trichodesmium erythraeum*. Aquat Ecol 58:1225–1236. https://doi.org/10.1007/s10452-024-10137-y
10. Hong H, Shen R, Zhang F, Wen Z, Chang S, Lin W, Kranz SA, Luo Y-W, Kao S-J, Morel FMM, Shi D. 2017. The complex effects of ocean acidification on the prominent N_2 -fixing cyanobacterium *Trichodesmium*. Science 356:527–531. https://doi.org/10.1126/science.aal2981
11. Zehr JP, Capone DG. 2020. Changing perspectives in marine nitrogen fixation. Science 368:eaay9514. https://doi.org/10.1126/science.aay9514
12. Zehr JP. 2011. Nitrogen fixation by marine cyanobacteria. Trends Microbiol 19:162–173. https://doi.org/10.1016/j.tim.2010.12.004
13. Berman-Frank I, Cullen JT, Shaked Y, Sherrell RM, Falkowski PG. 2001. Iron availability, cellular iron quotas, and nitrogen fixation in *Trichodesmium*. Limnol Oceanogr 46:1249–1260. https://doi.org/10.4319/lo.2001.46.6.1249
14. Shi T, Sun Y, Falkowski PG. 2007. Effects of iron limitation on the expression of metabolic genes in the marine cyanobacterium *Trichodesmium erythraeum* IMS101. Environ Microbiol 9:2945–2956. https://doi.org/10.1111/j.1462-2920.2007.01406.x
15. Küpper H, Šetlík I, Seibert S, Prášil O, Šetlikova E, Strittmatter M, Levitan O, Lohscheider J, Adamska I, Berman-Frank I. 2008. Iron limitation in the marine cyanobacterium *Trichodesmium* reveals new insights into regulation of photosynthesis and nitrogen fixation. New Phytol 179:784–798. https://doi.org/10.1111/j.1469-8137.2008.02497.x
16. Falkowski PG. 1997. Evolution of the nitrogen cycle and its influence on the biological sequestration of CO_2 in the ocean. Nature 387:272–275. https://doi.org/10.1038/387272a0
17. Wyatt NJ, Birchill A, Ussher S, Milne A, Bouman H, Troein ES, Pabortsava K, Wright A, Flanagan O, Bibby TS, Martin A, Moore CM. 2023. Phytoplankton responses to dust addition in the Fe–Mn co-limited eastern Pacific sub-Antarctic differ by source region. Proc Natl Acad Sci USA 120:e2220111120. https://doi.org/10.1073/pnas.2220111120
18. Morel FMM, Price NM. 2003. The biogeochemical cycles of trace metals in the oceans. Science 300:944–947. https://doi.org/10.1126/science.1083545
19. Boyd PW, Strzepek R, Takeda S, Jackson G, Wong CS, McKay RM, Law C, Kiyosawa H, Saito H, Sherry N, Johnson K, Gower J, Ramaiah N. 2005. The evolution and termination of an iron-induced mesoscale bloom in the northeast subarctic Pacific. Limnol Oceanogr 50:1872–1886. https://doi.org/10.4319/lo.2005.50.6.1872
20. Buesseler KO, Andrews JE, Pike SM, Charette MA. 2004. The effects of iron fertilization on carbon sequestration in the Southern Ocean. Science 304:414–417. https://doi.org/10.1126/science.1086895
21. Coale KH, Johnson KS, Fitzwater SE, Gordon RM, Tanner S, Chavez FP, Ferioli L, Sakamoto C, Rogers P, Millero F, Steinberg P, Nightingale P, Cooper D, Cochlan WP, Landry MR, Constantinou J, Rollwagen G, Trasvina A, Kudela R. 1996. A massive phytoplankton bloom induced by an ecosystem-scale iron fertilization experiment in the equatorial Pacific Ocean. Nature 383:495–501. https://doi.org/10.1038/383495a0
22. Martin JH, Coale KH, Johnson KS, Fitzwater SE, Gordon RM, Tanner SJ, Hunter CN, Elrod VA, Nowicki JL, Coley TL, et al. 1994. Testing the iron hypothesis in ecosystems of the equatorial Pacific Ocean. Nature 371:123–129. https://doi.org/10.1038/371123a0
23. Tsuda A, Takeda S, Saito H, Nishioka J, Nojiri Y, Kudo I, Kiyosawa H, Shiomoto A, Imai K, Ono T, et al. 2003. A mesoscale iron enrichment in

the western subarctic Pacific induces a large centric diatom bloom. Science 300:958–961. https://doi.org/10.1126/science.1082000
24. Achterberg EP, Moore CM, Henson SA, Steigenberger S, Stohl A, Eckhardt S, Avendano LC, Cassidy M, Hembury D, Klar JK, Lucas MI, Macey AI, Marsay CM, Ryan - Keogh TJ. 2013. Natural iron fertilization by the Eyjafjallajökull volcanic eruption. Geophys Res Lett 40:921–926. https://doi.org/10.1002/grl.50221
25. Bonnet S, Guieu C, Taillandier V, Boulart C, Bouruet-Aubertot P, Gazeau F, Scalabrin C, Bressac M, Knapp AN, Cuypers Y, González-Santana D, Forrer HJ, Grisoni J-M, Grosso O, Habasque J, Jardin-Camps M, Leblond N, Le Moigne FAC, Lebourges-Dhaussy A, Lory C, Nunige S, Pulido-Villena E, Rizzo AL, Sarthou G, Tilliette C. 2023. Natural iron fertilization by shallow hydrothermal sources fuels diazotroph blooms in the ocean. Science 380:812–817. https://doi.org/10.1126/science.abq4654
26. Olgun N, Duggen S, Croot PL, Delmelle P, Dietze H, Schacht U, Óskarsson N, Siebe C, Auer A, Garbe-Schönberg D. 2011. Surface ocean iron fertilization: the role of airborne volcanic ash from subduction zone and hot spot volcanoes and related iron fluxes into the Pacific Ocean. Global Biogeochem Cycles 25:n https://doi.org/10.1029/2009GB003761
27. Greene RM, Geider RJ, Falkowski PG. 1991. Effect of iron limitation on photosynthesis in a marine diatom. Limnol Oceanogr 36:1772–1782. https://doi.org/10.4319/lo.1991.36.8.1772
28. Price NM. 2005. The elemental stoichiometry and composition of an iron-limited diatom. Limnol Oceanogr 50:1159–1171. https://doi.org/10.4319/lo.2005.50.4.1159
29. Peacock MB, Kudela RM. 2014. Evidence for active vertical migration by two dinoflagellates experiencing iron, nitrogen, and phosphorus limitation. Limnol Oceanogr 59:660–673. https://doi.org/10.4319/lo.2014.59.3.0660
30. Reich HG, Rodriguez IB, LaJeunesse TC, Ho T-Y. 2020. Endosymbiotic dinoflagellates pump iron: differences in iron and other trace metal needs among the *Symbiodiniaceae*. Coral Reefs 39:915–927. https://doi.org/10.1007/s00338-020-01911-z
31. Segovia M, Lorenzo MR, Iñiguez C, García-Gómez C. 2018. Physiological stress response associated with elevated CO_2 and dissolved iron in a phytoplankton community dominated by the coccolithophore *Emiliania huxleyi*. Mar Ecol Prog Ser 586:73–89. https://doi.org/10.3354/meps12389
32. Schulz KG, Rost B, Burkhardt S, Riebesell U, Thoms S, Wolf-Gladrow DA. 2007. The effect of iron availability on the regulation of inorganic carbon acquisition in the coccolithophore *Emiliania huxleyi* and the significance of cellular compartmentation for stable carbon isotope fractionation. Geochim Cosmochim Acta 71:5301–5312. https://doi.org/10.1016/j.gca.2007.09.012
33. Fu F-X, Mulholland MR, Garcia NS, Beck A, Bernhardt PW, Warner ME, Sañudo-Wilhelmy SA, Hutchins DA. 2008. Interactions between changing pCO_2, N_2 fixation, and Fe limitation in the marine unicellular cyanobacterium *Crocosphaera*. Limnol Oceanog 53:2472–2484. https://doi.org/10.4319/lo.2008.53.6.2472
34. Garcia NS, Fu F, Sedwick PN, Hutchins DA. 2015. Iron deficiency increases growth and nitrogen-fixation rates of phosphorus-deficient marine cyanobacteria. ISME J 9:238–245. https://doi.org/10.1038/ismej.2014.104
35. Jacq V, Ridame C, L'Helguen S, Kaczmar F, Saliot A. 2014. Response of the unicellular diazotrophic cyanobacterium *Crocosphaera watsonii* to iron limitation. PLoS One 9:e86749. https://doi.org/10.1371/journal.pone.0086749
36. Yang N, Lin Y-A, Merkel CA, DeMers MA, Qu P-P, Webb EA, Fu F-X, Hutchins DA. 2022. Molecular mechanisms underlying iron and phosphorus co-limitation responses in the nitrogen-fixing cyanobacterium *Crocosphaera*. ISME J 16:2702–2711. https://doi.org/10.1038/s41396-022-01307-7
37. Cody GD, Boctor NZ, Filley TR, Hazen RM, Scott JH, Sharma A, Yoder HS. 2000. Primordial carbonylated iron-sulfur compounds and the synthesis of pyruvate. Science 289:1337–1340. https://doi.org/10.1126/science.289.5483.1337
38. Inomura K, Wilson ST, Deutsch C. 2019. Mechanistic model for the coexistence of nitrogen fixation and photosynthesis in marine *Trichodesmium*. mSystems 4:e00210-19. https://doi.org/10.1128/mSystems.00210-19
39. Berman-Frank I, Lundgren P, Chen Y-B, Küpper H, Kolber Z, Bergman B, Falkowski P. 2001. Segregation of nitrogen fixation and oxygenic photosynthesis in the marine cyanobacterium *Trichodesmium*. Science 294:1534–1537. https://doi.org/10.1126/science.1064082
40. Hania A, López-adams R, Prášil O, Eichner M. 2023. Protection of nitrogenase from photosynthetic O_2 evolution in *Trichodesmium*: methodological pitfalls and advances over 30 years of research. Photosynt 61:58–72. https://doi.org/10.32615/ps.2023.007
41. Sandh G, Xu L, Bergman B. 2012. Diazocyte development in the marine diazotrophic cyanobacterium *Trichodesmium*. Microbiology 158:345–352. https://doi.org/10.1099/mic.0.051268-0
42. Kelman D, Ben-Amotz A, Berman-Frank I. 2009. Carotenoids provide the major antioxidant defence in the globally significant N_2-fixing marine cyanobacterium *Trichodesmium*. Environ Microbiol 11:1897–1908. https://doi.org/10.1111/j.1462-2920.2009.01913.x
43. Küpper H, Andresen E, Wiegert S, Simek M, Leitenmaier B, Setlík I. 2009. Reversible coupling of individual phycobiliprotein isoforms during state transitions in the cyanobacterium *Trichodesmium* analysed by single-cell fluorescence kinetic measurements. Biochim Biophys Acta 1787:155–167. https://doi.org/10.1016/j.bbabio.2009.01.001
44. Held NA, Waterbury JB, Webb EA, Kellogg RM, McIlvin MR, Jakuba M, Valois FW, Moran DM, Sutherland KM, Saito MA. 2022. Dynamic diel proteome and daytime nitrogenase activity supports buoyancy in the cyanobacterium *Trichodesmium*. Nat Microbiol 7:300–311. https://doi.org/10.1038/s41564-021-01028-1
45. Blain S, Quéguiner B, Armand L, Belviso S, Bombled B, Bopp L, Bowie A, Brunet C, Brussaard C, Carlotti F, et al. 2007. Effect of natural iron fertilization on carbon sequestration in the Southern Ocean. Nature 446:1070–1074. https://doi.org/10.1038/nature05700
46. Polyviou D, Baylay AJ, Hitchcock A, Robidart J, Moore CM, Bibby TS. 2017. Desert dust as a source of iron to the globally important diazotroph *Trichodesmium* Front Microbiol 8:2683. https://doi.org/10.3389/fmicb.2017.02683
47. Snow JT, Polyviou D, Skipp P, Chrismas NAM, Hitchcock A, Geider R, Moore CM, Bibby TS. 2015. Quantifying integrated proteomic responses to iron stress in the globally important marine diazotroph *Trichodesmium*. PLoS One 10:e0142626. https://doi.org/10.1371/journal.pone.0142626
48. Snow JT, Schlosser C, Woodward EMS, Mills MM, Achterberg EP, Mahaffey C, Bibby TS, Moore CM. 2015. Environmental controls on the biogeography of diazotrophy and *Trichodesmium* in the Atlantic Ocean. Global Biogeochem Cycles 29:865–884. https://doi.org/10.1002/2015GB005090
49. Rubin M, Berman-Frank I, Shaked Y. 2011. Dust- and mineral-iron utilization by the marine dinitrogen-fixer *Trichodesmium*. Nature Geosci 4:529–534. https://doi.org/10.1038/ngeo1181
50. Tzubari Y, Magnezi L, Be'er A, Berman-Frank I. 2018. Iron and phosphorus deprivation induce sociality in the marine bloom-forming cyanobacterium *Trichodesmium*. ISME J 12:1682–1693. https://doi.org/10.1038/s41396-018-0073-5
51. Lommer M, Specht M, Roy A-S, Kraemer L, Andreson R, Gutowska MA, Wolf J, Bergner SV, Schilhabel MB, Klostermeier UC, Beiko RG, Rosenstiel P, Hippler M, LaRoche J. 2012. Genome and low-iron response of an oceanic diatom adapted to chronic iron limitation. Genome Biol 13:R66. https://doi.org/10.1186/gb-2012-13-7-r66
52. Behrenfeld MJ, Milligan AJ. 2013. Photophysiological expressions of iron stress in phytoplankton. Annu Rev Mar Sci 5:217–246. https://doi.org/10.1146/annurev-marine-121211-172356
53. Zhang F, Hong H, Kranz SA, Shen R, Lin W, Shi D. 2019. Proteomic responses to ocean acidification of the marine diazotroph *Trichodesmium* under iron-replete and iron-limited conditions. Photosynth Res 142:17–34. https://doi.org/10.1007/s11120-019-00643-8
54. Cerdan-Garcia E, Baylay A, Polyviou D, Woodward EMS, Wrightson L, Mahaffey C, Lohan MC, Moore CM, Bibby TS, Robidart JC. 2022. Transcriptional responses of *Trichodesmium* to natural inverse gradients of Fe and P availability. ISME J 16:1055–1064. https://doi.org/10.1038/s41396-021-01151-1
55. Held NA, Webb EA, McIlvin MM, Hutchins DA, Cohen NR, Moran DM, Kunde K, Lohan MC, Mahaffey C, Woodward EMS, Saito MA. 2020. Co-occurrence of Fe and P stress in natural populations of the marine diazotroph *Trichodesmium*. Biogeosciences 17:2537–2551. https://doi.org/10.5194/bg-17-2537-2020
56. Walworth NG, Fu F-X, Webb EA, Saito MA, Moran D, McIlvin MR, Lee MD, Hutchins DA. 2016. Mechanisms of increased *Trichodesmium* fitness under iron and phosphorus co-limitation in the present and future ocean. Nat Commun 7:12081. https://doi.org/10.1038/ncomms12081

57. Hutchins DA, Boyd PW. 2016. Marine phytoplankton and the changing ocean iron cycle. Nature Clim Change 6:1072–1079. https://doi.org/10.1038/nclimate3147
58. Hutchins DA, Capone DG. 2022. The marine nitrogen cycle: new developments and global change. Nat Rev Microbiol 20:401–414. https://doi.org/10.1038/s41579-022-00687-z
59. Shi D, Xu Y, Hopkinson BM, Morel FMM. 2010. Effect of ocean acidification on iron availability to marine phytoplankton. Science 327:676–679. https://doi.org/10.1126/science.1183517
60. Chappell PD, Webb EA. 2010. A molecular assessment of the iron stress response in the two phylogenetic clades of *Trichodesmium*. Environ Microbiol 12:13–27. https://doi.org/10.1111/j.1462-2920.2009.02026.x
61. Walworth N, Pfreundt U, Nelson WC, Mincer T, Heidelberg JF, Fu F, Waterbury JB, Glavina del Rio T, Goodwin L, Kyrpides NC, Land ML, Woyke T, Hutchins DA, Hess WR, Webb EA. 2015. *Trichodesmium* genome maintains abundant, widespread noncoding DNA in situ, despite oligotrophic lifestyle. Proc Natl Acad Sci USA 112:4251–4256. https://doi.org/10.1073/pnas.1422332112
62. Burén S, Jiménez-Vicente E, Echavarri-Erasun C, Rubio LM. 2020. Biosynthesis of nitrogenase cofactors. Chem Rev 120:4921–4968. https://doi.org/10.1021/acs.chemrev.9b00489
63. Shi T, Ilikchyan I, Rabouille S, Zehr JP. 2010. Genome-wide analysis of diel gene expression in the unicellular N_2-fixing cyanobacterium *Crocosphaera watsonii* WH 8501. ISME J 4:621–632. https://doi.org/10.1038/ismej.2009.148
64. Bothe H, Tennigkeit J, Eisbrenner G. 1977. The utilization of molecular hydrogen by the blue-green alga *Anabaena cylindrica*. Arch Microbiol 114:43–49. https://doi.org/10.1007/BF00429628
65. Tamagnini P, Leitão E, Oliveira P, Ferreira D, Pinto F, Harris DJ, Heidorn T, Lindblad P. 2007. Cyanobacterial hydrogenases: diversity, regulation and applications. FEMS Microbiol Rev 31:692–720. https://doi.org/10.1111/j.1574-6976.2007.00085.x
66. Niyogi KK, Wolosiuk RA, Malkin R. 2015. Photosynthesis, p 508–566. In Buchanan BB, Gruissem W, Jones RL (ed), Biochemistry and molecular biology of plants. John Wiley & Sons, Ltd, New York, NY.
67. Bench SR, Heller P, Frank I, Arciniega M, Shilova IN, Zehr JP. 2013. Whole genome comparison of six *Crocosphaera watsonii* strains with differing phenotypes. J Phycol 49:786–801. https://doi.org/10.1111/jpy.12090
68. Shen G, Gan F, Bryant DA. 2016. The siderophilic cyanobacterium *Leptolyngbya* sp. strain JSC-1 acclimates to iron starvation by expressing multiple *isiA*-family genes. Photosynth Res 128:325–340. https://doi.org/10.1007/s11120-016-0257-7
69. Chen HYS, Bandyopadhyay A, Pakrasi HB. 2018. Function, regulation and distribution of IsiA, a membrane-bound chlorophyll a-antenna protein in cyanobacteria. Photosynt 56:322–333. https://doi.org/10.1007/s11099-018-0787-7
70. La Roche J, van der Staay GW, Partensky F, Ducret A, Aebersold R, Li R, Golden SS, Hiller RG, Wrench PM, Larkum AW, Green BR. 1996. Independent evolution of the prochlorophyte and green plant chlorophyll *a/b* light-harvesting proteins. Proc Natl Acad Sci USA 93:15244–15248. https://doi.org/10.1073/pnas.93.26.15244
71. Nagao R, Kato K, Hamaguchi T, Ueno Y, Tsuboshita N, Shimizu S, Furutani M, Ehira S, Nakajima Y, Kawakami K, Suzuki T, Dohmae N, Akimoto S, Yonekura K, Shen J-R. 2023. Structure of a monomeric photosystem I core associated with iron-stress-induced-A proteins from *Anabaena* sp. PCC 7120. Nat Commun 14:920. https://doi.org/10.1038/s41467-023-36504-1
72. Bibby TS, Nield J, Barber J. 2001. Iron deficiency induces the formation of an antenna ring around trimeric photosystem I in cyanobateria. Nature 412:743–745. https://doi.org/10.1038/35089098
73. Kouřil R, Yeremenko N, D'Haene S, Oostergetel GT, Matthijs HCP, Dekker JP, Boekema EJ. 2005. Supercomplexes of IsiA and photosystem I in a mutant lacking subunit PsaL. Biochim Biophys Acta Bioenerget 1706:262–266. https://doi.org/10.1016/j.bbabio.2004.11.008
74. Hewson I, Poretsky RS, Beinart RA, White AE, Shi T, Bench SR, Moisander PH, Paerl RW, Tripp HJ, Montoya JP, Moran MA, Zehr JP. 2009. *In situ* transcriptomic analysis of the globally important keystone N_2-fixing taxon *Crocosphaera watsonii* . ISME J 3:618–631. https://doi.org/10.1038/ismej.2009.8
75. Olsen MT, Nowack S, Wood JM, Becraft ED, LaButti K, Lipzen A, Martin J, Schackwitz WS, Rusch DB, Cohan FM, Bryant DA, Ward DM. 2015. The molecular dimension of microbial species: 3. Comparative genomics of *Synechococcus* strains with different light responses and in situ diel transcription patterns of associated putative ecotypes in the Mushroom Spring microbial mat. Front Microbiol 6:604. https://doi.org/10.3389/fmicb.2015.00604
76. Clarke AK, Soitamo A, Gustafsson P, Oquist G. 1993. Rapid interchange between two distinct forms of cyanobacterial photosystem II reaction-center protein D1 in response to photoinhibition. Proc Natl Acad Sci USA 90:9973–9977. https://doi.org/10.1073/pnas.90.21.9973
77. Mulo P, Sicora C, Aro EM. 2009. Cyanobacterial *psbA* gene family: optimization of oxygenic photosynthesis. Cell Mol Life Sci 66:3697–3710. https://doi.org/10.1007/s00018-009-0103-6
78. Allen AE, Moustafa A, Montsant A, Eckert A, Kroth PG, Bowler C. 2012. Evolution and functional diversification of fructose bisphosphate aldolase genes in photosynthetic marine diatoms. Mol Biol Evol 29:367–379. https://doi.org/10.1093/molbev/msr223
79. Peers GS. 2005. Increased metabolic requirements for manganese and copper in iron-limited marine diatoms. Doctoral dissertation. McGill University, Montreal, Canada.
80. Marsh HV, Evans HJ, Matrone G. 1963. Investigations of the role of iron in chlorophyll metabolism I. Effect of iron deficiency on chlorophyll and heme content and on the activities of certain enzymes in leaves. Plant Physiol 38:632–638. https://doi.org/10.1104/pp.38.6.632
81. Kroh GE, Pilon M. 2020. Regulation of iron homeostasis and use in chloroplasts. Int J Mol Sci 21:3395. https://doi.org/10.3390/ijms21093395
82. Facey JA, King JJ, Apte SC, Mitrovic SM. 2022. Assessing the importance of cobalt as a micronutrient for freshwater cyanobacteria. J Phycol 58:71–79. https://doi.org/10.1111/jpy.13216
83. Bertrand EM, Moran DM, McIlvin MR, Hoffman JM, Allen AE, Saito MA. 2013. Methionine synthase interreplacement in diatom cultures and communities: implications for the persistence of B_{12} use by eukaryotic phytoplankton. Limnol Oceanogr 58:1431–1450. https://doi.org/10.4319/lo.2013.58.4.1431
84. Hawco NJ, McIlvin MM, Bundy RM, Tagliabue A, Goepfert TJ, Moran DM, Valentin-Alvarado L, DiTullio GR, Saito MA. 2020. Minimal cobalt metabolism in the marine cyanobacterium *Prochlorococcus*. Proc Natl Acad Sci USA 117:15740–15747. https://doi.org/10.1073/pnas.2001393117
85. Walworth NG, Lee MD, Suffridge C, Qu P, Fu F-X, Saito MA, Webb EA, Sañudo-Wilhelmy SA, Hutchins DA. 2018. Functional genomics and phylogenetic evidence suggest genus-wide cobalamin production by the globally distributed marine nitrogen fixer *Trichodesmium*. Front Microbiol 9:189. https://doi.org/10.3389/fmicb.2018.00189
86. Sevilla E, Bes MT, Peleato ML, Fillat MF. 2021. Fur-like proteins: beyond the ferric uptake regulator (Fur) paralog. Arch Biochem Biophys 701:108770. https://doi.org/10.1016/j.abb.2021.108770
87. Lee J-W, Helmann JD. 2006. The PerR transcription factor senses H_2O_2 by metal-catalysed histidine oxidation. Nature 440:363–367. https://doi.org/10.1038/nature04537
88. Riediger M, Hernández-Prieto MA, Song K, Hess WR, Futschik ME. 2021. Genome-wide identification and characterization of Fur-binding sites in the cyanobacteria *Synechocystis* sp. PCC 6803 and PCC 6714. DNA Res 28:dsab023. https://doi.org/10.1093/dnares/dsab023
89. Hernández JA, López-Gomollón S, Bes MT, Fillat MF, Peleato ML. 2004. Three fur homologues from *Anabaena* sp. PCC7120: exploring reciprocal protein-promoter recognition. FEMS Microbiol Lett 236:275–282. https://doi.org/10.1016/j.femsle.2004.05.050
90. Johnson DC, Dean DR, Smith AD, Johnson MK. 2005. Structure, function, and formation of biological iron-sulfur clusters. Annu Rev Biochem 74:247–281. https://doi.org/10.1146/annurev.biochem.74.082803.133518
91. González A, Bes MT, Valladares A, Peleato ML, Fillat MF. 2012. FurA is the master regulator of iron homeostasis and modulates the expression of tetrapyrrole biosynthesis genes in Anabaena sp. PCC 7120. Environ Microbiol 14:3175–3187. https://doi.org/10.1111/j.1462-2920.2012.02897.x
92. Yuvaniyama P, Agar JN, Cash VL, Johnson MK, Dean DR. 2000. NifS-directed assembly of a transient [2Fe-2S] cluster within the NifU protein. Proc Natl Acad Sci USA 97:599–604. https://doi.org/10.1073/pnas.97.2.599
93. Dos Santos PC, Dean DR, Hu Y, Ribbe MW. 2004. Formation and insertion of the nitrogenase iron-molybdenum cofactor. Chem Rev 104:1159–1173. https://doi.org/10.1021/cr020608l
94. Nachin L, Loiseau L, Expert D, Barras F. 2003. SufC: an unorthodox cytoplasmic ABC/ATPase required for [Fe—S] biogenesis under

oxidative stress. EMBO J 22:427–437. https://doi.org/10.1093/emboj/cdg061
95. Vuorijoki L, Tiwari A, Kallio P, Aro E-M. 2017. Inactivation of iron-sulfur cluster biogenesis regulator SufR in *Synechocystis* sp. PCC 6803 induces unique iron-dependent protein-level responses. Biochim Biophys Acta Gen Subj 1861:1085–1098. https://doi.org/10.1016/j.bbagen.2017.02.020
96. Wang T, Shen G, Balasubramanian R, McIntosh L, Bryant DA, Golbeck JH. 2004. The *sufR* gene (*sll0088* in *Synechocystis* sp. strain PCC 6803) functions as a repressor of the *sufBCDS* operon in iron-sulfur cluster biogenesis in cyanobacteria. J Bacteriol 186:956–967. https://doi.org/10.1128/JB.186.4.956-967.2004
97. Massé E, Gottesman S. 2002. A small RNA regulates the expression of genes involved in iron metabolism in *Escherichia coli*. Proc Natl Acad Sci USA 99:4620–4625. https://doi.org/10.1073/pnas.032066599
98. Georg J, Kostova G, Vuorijoki L, Schön V, Kadowaki T, Huokko T, Baumgartner D, Müller M, Klähn S, Allahverdiyeva Y, Hihara Y, Futschik ME, Aro E-M, Hess WR. 2017. Acclimation of oxygenic photosynthesis to iron starvation is controlled by the sRNA IsaR1. Curr Biol 27:1425–1436. https://doi.org/10.1016/j.cub.2017.04.010
99. Kunert A, Vinnemeier J, Erdmann N, Hagemann M. 2003. Repression by Fur is not the main mechanism controlling the iron-inducible *isiAB* operon in the cyanobacterium *Synechocystis* sp. PCC 6803. FEMS Microbiol Lett 227:255–262. https://doi.org/10.1016/S0378-1097(03)00689-X
100. Riediger M, Kadowaki T, Nagayama R, Georg J, Hihara Y, Hess WR. 2019. Biocomputational analyses and experimental validation identify the regulon controlled by the redox-responsive transcription factor RpaB. iScience 15:316–331. https://doi.org/10.1016/j.isci.2019.04.033
101. Chagneau CV, Payros D, Tang-Fichaux M, Auvray F, Nougayrède J-P, Oswald E. 2022. The pks island: a bacterial Swiss army knife? Colibactin: beyond DNA damage and cancer. Trends Microbiol 30:1146–1159. https://doi.org/10.1016/j.tim.2022.05.010
102. Silpe JE, Wong JWH, Owen SV, Baym M, Balskus EP. 2022. The bacterial toxin colibactin triggers prophage induction. Nature 603:315–320. https://doi.org/10.1038/s41586-022-04444-3
103. Lee MD, Walworth NG, McParland EL, Fu F-X, Mincer TJ, Levine NM, Hutchins DA, Webb EA. 2017. The *Trichodesmium consortium*: conserved heterotrophic co-occurrence and genomic signatures of potential interactions. ISME J 11:1813–1824. https://doi.org/10.1038/ismej.2017.49
104. Sheridan CC. 2002. The microbial and metazoan community associated with colonies of *Trichodesmium* spp.: a quantitative survey. J Plankton Res 24:913–922. https://doi.org/10.1093/plankt/24.9.913
105. Basu S, Matondkar SGP, Furtado I. 2011. Enumeration of bacteria from a *Trichodesmium* spp. bloom of the Eastern Arabian Sea: elucidation of their possible role in biogeochemistry. J Appl Phycol 23:309–319. https://doi.org/10.1007/s10811-010-9589-4
106. Koedooder C, Zhang F, Wang S, Basu S, Haley ST, Tolic N, Nicora CD, Glavina Del Rio T, Dyhrman ST, Gledhill M, Boiteau RM, Rubin-Blum M, Shaked Y. 2023. Taxonomic distribution of metabolic functions in bacteria associated with *Trichodesmium* consortia. mSystems 8:e00742-23. https://doi.org/10.1128/msystems.00742-23
107. Walworth NG, Lee MD, Dolzhenko E, Fu F-X, Smith AD, Webb EA, Hutchins DA. 2021. Long-term m5C methylome dynamics parallel phenotypic adaptation in the cyanobacterium *Trichodesmium*. Mol Biol Evol 38:927–939. https://doi.org/10.1093/molbev/msaa256
108. Teikari J, Österholm J, Kopf M, Battchikova N, Wahlsten M, Aro E-M, Hess WR, Sivonen K. 2015. Transcriptomic and proteomic profiling of *Anabaena* sp. strain 90 under inorganic phosphorus stress. Appl Environ Microbiol 81:5212–5222. https://doi.org/10.1128/AEM.01062-15
109. Shi D, Kranz SA, Kim JM, Morel FMM. 2012. Ocean acidification slows nitrogen fixation and growth in the dominant diazotroph *Trichodesmium* under low-iron conditions. Proc Natl Acad Sci USA 109:E3094–100. https://doi.org/10.1073/pnas.1216012109
110. Richier S, Macey AI, Pratt NJ, Honey DJ, Moore CM, Bibby TS. 2012. Abundances of iron-binding photosynthetic and nitrogen-fixing proteins of *Trichodesmium* both in culture and in situ from the North Atlantic. PLoS One 7:e35571. https://doi.org/10.1371/journal.pone.0035571
111. Jassby AD, Platt T. 1976. Mathematical formulation of the relationship between photosynthesis and light for phytoplankton. Limnol Oceanogr 21:540–547. https://doi.org/10.4319/lo.1976.21.4.0540
112. Capone DG. 2018. Determination of nitrogenase activity in aquatic samples using the acetylene reduction procedure, p 621–631. In Kemp Paul F, Sherr Barry F, Sherr Evelyn B, Cole Jonathan J (ed), Handbook of methods in aquatic microbial ecology. CRC Press, Boca Raton, FL.
113. Chen L, Xu J, Wang T, Huang Y, Yuan D, Gong Z. 2021. Toward a versatile flow technique: development and application of reverse flow dual-injection analysis (rFDIA) for determining dissolved iron redox species and soluble reactive phosphorus in seawater. Talanta 232:122404. https://doi.org/10.1016/j.talanta.2021.122404
114. Johansson K-E, Heldtander MUK, Pettersson B. 1998. Characterization of mycoplasmas by PCR and sequence analysis with universal 16S rDNA primers, p 145–165. In Miles Roger, Nicholas Robin (ed), Mycoplasma Protocols: Methods in Molecular Biology, Volume 104. Humana Press, Totowa, NJ.
115. Livak KJ, Schmittgen TD. 2001. Analysis of relative gene expression data using real-time quantitative PCR and the $2^{-\Delta\Delta C_T}$ method. Methods 25:402–408. https://doi.org/10.1006/meth.2001.1262
116. Didion JP, Martin M, Collins FS. 2017. Atropos: specific, sensitive, and speedy trimming of sequencing reads. PeerJ 5:e3720. https://doi.org/10.7717/peerj.3720
117. Andrews S. 2010. FastQC. A Quality control tool for high throughput sequence data. Available from: http://wwwbioinformaticsbabrahamacuk/projects/fastqc
118. Kopylova E, Noé L, Touzet H. 2012. SortMeRNA: fast and accurate filtering of ribosomal RNAs in metatranscriptomic data. Bioinformatics 28:3211–3217. https://doi.org/10.1093/bioinformatics/bts611
119. Li H. 2013. Aligning sequence reads, clone sequences and assembly contigs with BWA-MEM. arXiv:13033997.
120. Liao Y, Smyth GK, Shi W. 2014. featureCounts: an efficient general purpose program for assigning sequence reads to genomic features. Bioinformatics 30:923–930. https://doi.org/10.1093/bioinformatics/btt656
121. Love MI, Huber W, Anders S. 2014. Moderated estimation of fold change and dispersion for RNA-seq data with DESeq2. Genome Biol 15:550. https://doi.org/10.1186/s13059-014-0550-8
122. Robinson MD, McCarthy DJ, Smyth GK. 2010. edgeR: a Bioconductor package for differential expression analysis of digital gene expression data. Bioinformatics 26:139–140. https://doi.org/10.1093/bioinformatics/btp616
123. Falcon S, Gentleman R. 2007. Using GOstats to test gene lists for GO term association. Bioinformatics 23:257–258. https://doi.org/10.1093/bioinformatics/btl567
124. Yu G, Wang L-G, Han Y, He Q-Y. 2012. clusterProfiler: an R package for comparing biological themes among gene clusters. OMICS 16:284–287. https://doi.org/10.1089/omi.2011.0118
125. Katoh K, Standley DM. 2013. MAFFT multiple sequence alignment software version 7: improvements in performance and usability. Mol Biol Evol 30:772–780. https://doi.org/10.1093/molbev/mst010
126. Capella-Gutiérrez S, Silla-Martínez JM, Gabaldón T. 2009. trimAl: a tool for automated alignment trimming in large-scale phylogenetic analyses. Bioinformatics 25:1972–1973. https://doi.org/10.1093/bioinformatics/btp348
127. Naser-Khdour S, Quang Minh B, Lanfear R. 2022. Assessing confidence in root placement on phylogenies: an empirical study using nonreversible models for mammals.. Syst Biol 71:959–972. https://doi.org/10.1093/sysbio/syab067
128. Kalyaanamoorthy S, Minh BQ, Wong TKF, von Haeseler A, Jermiin LS. 2017. ModelFinder: fast model selection for accurate phylogenetic estimates. Nat Methods 14:587–589. https://doi.org/10.1038/nmeth.4285